

# An investigation into the effect of pressure source parameters and water depth on the wake wash wave generated by moving pressure source

*Mohammadreza Javanmardi<sup>1</sup>*

Adjunct Assistant Professor, Sharif University of technology, Tehran, Iran

*Jonathan Binns*

Associate Dean of Research, Australian Maritime College, Launceston, Tasmania, Australia, 7250

*Giles Thomas*

Professor, University College London, Torrington Place, London WC1E 7JE, UK

*Martin Renilson*

Adjunct Professor, University of Tasmania, Launceston, Tasmania, Australia, 7250

## Abstract

In this study the effect of moving pressure source and channel parameters on the generated waves in a channel was numerically investigated. Draught, angle of attack and profile shape were investigated as parameters of pressure source and water depth and blockage factor as channel parameters on wave height. Firstly, the chosen Computational Fluid Dynamics (CFD) approach was validated with the experimental data over a range of speed. Then the CFD study was conducted for further investigations. It was shown that that by enlarging draught, angle of attack and beam of the pressure source, the wave height generated will be increased. Channel study showed that it is possible to increase the wave height generated by shallowing water for a given speed as long as the depth Froude number is subcritical and the wave height generated is independent of water depth for supercritical depth Froude numbers. The blockage factor has more influence at supercritical Froude depth values, while at subcritical Froude values is negligible compare with water depth.

## Keywords

Wake wash, wave propagation, Computational Fluid dynamics, Towing Tank, Pressure Source

## Introduction

The wake pattern which is produced by a moving point across the surface of deep water was first explained mathematically by Lord Kelvin (William Thomson) [1] and is known as the Kelvin wake pattern. All vessels operating in deep water produce a Kelvin type wave pattern consisting of two

---

<sup>1</sup> Corresponding author

Email: [mj00@utas.edu.au](mailto:mj00@utas.edu.au)

Fax: +982166165563

Present address: Marine Lab., Sharif University of Technology, Tehran, Iran

1 kinds of waves: transverse waves which crest across the ship track and divergent waves which crests  
2 roughly parallel to the ship track, moving outward. The waves are confined to a wedge shaped region  
3 behind the ship, and the half angle of the wedge is 19.5 degrees. This angle is independent of the ship  
4 speed as long as the deep water condition is satisfied.

5 Many studies have been conducted into the effect of waves on vessels operating in shallow and  
6 restricted waterways, for example [2, 3]. In addition, significant research has been conducted into  
7 wash wave impacts on ecology and the environment, and vessel operation in shallow water close to  
8 the coastline [4].

9 The wash waves generated by vessels can be also characterized in terms of the hull shape [5] and  
10 operating condition [6]. Due to the great interest in wake wash effects, a considerable amount of  
11 research effort has been conducted in recent years. In model experimental studies the focus has been  
12 on designing low-wash ships and acquiring reliable data for validation [7-9].

13 Most research has been conducted using theoretical [10] or experimental [11, 12] approaches. For a  
14 ship moving in water of uniform depth, linear and nonlinear theories can be applied usefully in the  
15 subcritical and the supercritical speed range [13, 14]. Thin ship theory can be used for the wave  
16 generation by a ship moving in a channel. This theory provides an alternative to higher order panel  
17 methods for estimating wave resistance when applied solely to slender hulls [10], but it is not valid for  
18 unsteady cases and transom stern flow separation [13]. More general shallow-water approximations  
19 are obtained from Boussinesq type equations, which are valid for most arbitrarily unsteady cases.  
20 Boussinesq's equations based on a suitable reference level were used for computing ship waves in  
21 shallow water. However this method is not able to predict the 3D flow pattern around the vessel [15].  
22 An alternative is to combine the thin ship theory and the Boussinesq method. This hybrid approach  
23 combines a steady nonlinear panel method for the near-ship flow with a Boussinesq solver for the far-  
24 field wave propagation [13]. However, this method is only useful for steady problems. It should be  
25 noted that due to the nonlinear and unsteady nature, as well as the large domain feature of the wash  
26 problems, they can be neither solved well by the linear wave theory nor approximated efficiently by  
27 nonlinear singularity methods. Typically, the finite volume method has been used to predict the wave  
28 generated and its propagation [15, 16]. Previous studies by the authors showed that the numerical  
29 approach can predict wave propagation accurately [17, 18].

30 In the present study, a pressure source model was tested at Australian Maritime College Towing Tank  
31 at different speed and the generated waves parameters were captured by wave probes. Next, the  
32 simulations were conducted by ANSYS-Fluent software version 14.5 in same condition as the  
33 experimental. Through the comparison of computed and measured results, applicability of the  
34 numerical method is examined. Subsequently the numerical approach was used for further  
35 investigation.

## 1 **Experimental setup**

2 In order to generate waves, a moving wanedozer model was used as a pressure source during the  
3 experimental. The wanedozer model [19] is a wedge shape model with the constant beam (Figure ).  
4 The main particulars of the wanedozer are listed in Table .

5 This model was tested at the Australian Maritime College towing tank which has a length of 100m,  
6 and a width of 3.5m. The water depth for the tests was 1.5m in all conducted tests. Three wave probes  
7 were positioned at 0.75, 1.0 and 1.25 m from the centre-line of the model to record the wave  
8 parameters (Figure ), where  $y^*$  is defined by the distance of the wave probe position over the width of  
9 the channel ( $y^* = y/W$ ). Two load cells were installed on the model to measure the vertical and drag  
10 forces. The model was tested at various depth Froude numbers from 0.43 to 0.99.

## 11 **Numerical simulation**

12 The CFD software ANSYS-Fluent version 14.5 was used as the flow solver [20]. The governing  
13 equations are three-dimensional Reynolds Averaged Navier-Stokes equations for incompressible  
14 flows. The Volume of Fluid (VOF) approach was used with a time-dependent and explicit time  
15 discretization scheme employed to solve the equations. The SIMPLE algorithm was used for the  
16 pressure-velocity coupling and the PRESTO scheme for the pressure interpolation. The k-epsilon  
17 model with the standard wall function was utilized for turbulence modelling. The 2<sup>nd</sup> order upwind  
18 scheme was used for solving the momentum equations and the High Resolution Interface Capturing  
19 scheme (HRIC) for the solution of the volume fraction equations.

20 Figure 34 shows the computational grid domain. For the numerical investigation, a domain  
21 comprising 6m in front of the model and 13.5m behind it was considered. The heave and trim were  
22 fixed at the same value as used in experimental tests. As the flow has a plane of symmetry about the  
23 centre plane, to decrease the processing time, half of the domain was used. The origin of the  
24 coordinate system was located at the middle of the model. The open channel boundary condition was  
25 used to specify the inlet and outlet boundary condition. Inlet velocity and outflow boundary  
26 conditions were selected for inlet and outlet boundaries respectively. A symmetry plane was used  
27 along the centre plane, and the remaining boundary surfaces along the exterior of the domain were set  
28 to no-slip wall conditions. The more details about mesh domain and cells' properties are presented in  
29 (21).

## 1 **Validating the numerical approach**

2 The results of the numerical simulation have been compared with experimental data in various  
3 figures. Figure shows the drag coefficient results for the experimental and numerical investigations,  
4 and Figure presents the vertical force (or lift) coefficient for different speeds. Drag and vertical force  
5 coefficients are defined as:

$$C_d = \frac{\text{Drag}}{0.5 \times \rho \times V^2 \times D \times B} \quad (1)$$

$$C_l = \frac{\text{Vertical Force}}{0.5 \times \rho \times V^2 \times LWL \times B}$$

6

7 Where  $\rho$  is water density,  $V$  is speed of the pressure source,  $D$  is draught,  $B$  is beam and  $LWL$  is  
8 length of waterline. It should be mentioned, the water separates from model sides during tests and  
9 only model bottom remains wet (21). In addition, the highest portion of total drag (95%) can be  
10 attributed to pressure drag (21). Therefore, in Equation 1, the area is equal  $D \times B$  and in Equation 2,  
11 the area is equal  $LWL \times B$ . The standard error bars (5%) were shown for all the experimental data.

12 It is clear that the simulation results are in good agreement with the experimental data with respect to  
13 the forces. The percentage variations between numerical results and the experimental data are mostly  
14 less than 5%. To increase the accuracy of the results for lower speed, the mesh should be refined,  
15 however in this study the higher speeds are more interested. The free-surface elevation for depth  
16 Froude numbers 0.7 and 0.99 for nearest, middle and farthest wave probes are presented in Figure to  
17 Figure . Free-surface elevations show the Fluent software is able to predict the wave patterns at  
18 different lateral distances. According to presented results, the numerical method is validated, and can  
19 be used to investigate the effects of changes in parameters. It should be mentioned that first wave  
20 behind the pressure source was considered as surfable wave, therefore surface elevation of the first  
21 wave behind the pressure source was considered and as soon as the first wave reached to steady state,  
22 the simulations were stopped. To improve the accuracy of the results in far filed the simulation time  
23 should be increased and mesh should be refined, however in this study was unnecessary.

24

## 25 **Investigating the effect of various parameters**

### 26 **Pressure source parameters**

27 Draught, beam and angle of attack are the main parameters of the wadedozer which were numerically  
28 investigated with respect to the wave generated height and propagation. Changing any of these

parameters will alter the wadedozer's displacement. In this study, only one of the parameters was changed at a time and the rest kept constant in order to compare the numerical results and examine the effect of the changed parameter.

#### Draught

	<b>Draught (m)</b>	<b>Beam (m)</b>	<b>Angle of attack (deg)</b>	<b>LWL (m)</b>	<b>Displacement (m<sup>3</sup>)</b>	<b>Blockage factor</b>
<b>Model 1</b>	0.1	0.3	14	0.40	0.006015	0.0057
<b>Model 2</b>	0.12	0.3	14	0.48	0.00866	0.0068

Table shows the dimensions of two wadedozers. Model 1 is the model which was used in the experimental tests and the previous simulations. To consider the effect of draught on generated waves, a new model (Model 2) was simulated. The draught of Model 2 was 20% more than Model 1. These simulations were conducted in deep water condition (1.5 m water depth). Since the tests were conducted in 1.5 m water depth, the draught change does not have a significant influence on the blockage factor. Blockage factor can be defined as:

$$\text{Blockage factor } (\kappa) = \frac{\text{Model cross section area } (A_s)}{\text{Channel cross section area } (A_c)} \quad (3)$$

The comparison between Model 1 and Model 2 shows that increasing the draught causes an increase in wave height. It is predicted there is a specific draught which generated wave starts to break and increasing draught more, does not have effect on the generated wave height. Figure to Figure present the wave heights comparison for two different models at different lateral distances, where  $y$  is lateral distance,  $B$  and  $W$  are model and channel widths respectively,  $H$  is wave height of first wave behind the pressure source and  $h$  is water depth.

#### Angle of attack

Another potentially important parameter is the angle of attack. The angle of attack is the angle between the entry surface and the water surface. The previous studies were conducted with a wadedozer with a 14 degree angle of attack. The 14 degree angle of attack was presented as the optimum angle in [19]. In this study, wadedozers with different angles of attack were simulated. By altering the angle of attack, the length of water line (LWL) and the displacement will be changed and

1 the draught and beam remained constant. The wadedozer with the lowest angle of attack has the  
 2 largest displacement and vice versa.

	<b>Draught (m)</b>	<b>Beam (m)</b>	<b>Angle of attack (deg.)</b>	<b>LWL (m)</b>	<b>Displacement (m<sup>3</sup>)</b>	<b>Blockage factor</b>
<b>Model 1</b>	0.1	0.3	14	0.401	0.006015	0.0057
<b>Model 3</b>	0.1	0.3	10	0.567	0.008505	0.0057
<b>Model 4</b>	0.1	0.3	7	0.814	0.01221	0.0057
<b>Model 5</b>	0.1	0.3	4	1.43	0.02145	0.0057

3  
 4 Table presents the wadedozers parameters. Figure to Figure illustrate the wave heights for different  
 5 wadedozers at different  $Fr_h$ .

6 By decreasing the angle of attack, the variation of wave height with lateral distances decreases. For  
 7 example, for Model 5 (angle of attack of 4 degree) at  $Fr_h = 0.9$ , the wave height is almost constant  
 8 for the entire width of the channel. By increasing the angle of attack, the maximum wave height is  
 9 increased due to increasing the pressure gradient. It can be said that  $\frac{D}{LWL} \propto \frac{\delta p}{\delta x}$ , where  $\frac{\delta p}{\delta x}$  is pressure  
 10 gradient in longitudinal direction ( $p$  is pressure force). Therefore by increasing the angle of attack for  
 11 constant draught (D) the length of waterline (LWL) will decrease. Therefore, the pressure gradient  
 12 will increase, and as a consequence, the wave generated height will increase. Model 5 has the largest  
 13 displacement while it generates the lowest wave height. Increasing the displacement by changing the  
 14 angle of attack (or LWL) has the opposite effect on wave height. By decreasing the angle of attack the  
 15 model drag decreases. Figure and Figure show the drag and vertical forces for different angle of  
 16 attack. The highest portion of total drag can be attributed to pressure drag (21). Increasing the angle of  
 17 attack increases the pressure drag and decreasing the angle of attack increases the wetted area and as a  
 18 result increases the viscous drag. It can be concluded that Model 5 with the largest displacement  
 19 generates the lowest wave height because it has minimum pressure drag, and Model 1 with lowest  
 20 displacement generated the highest wave height because it has maximum drag.

## 21 **Beam**

22 The effect of pressure source beam on the generated wave height and quality was investigated. For  
 23 this investigation, the wadedozer beam was increased from 300mm (model 1) to 433mm (model 6). In  
 24 addition, it should be noted that the wadedozer with 433mm beam (Model 6) has the same  
 25 displacement as the model with 120mm draught (model 2) which was used previously for the draught  
 26 investigation.

	Draught (m)	Beam (m)	LWL (m)	Water plane (m <sup>2</sup> )	Angle of attack (degree)	Volume displacement (m <sup>3</sup> )
Model 1	0.1	0.3	0.40	0.120	14	0.006
Model 2	0.12	0.3	0.48	0.144	14	0.00866
Model 6	0.1	0.433	0.40	0.174	14	0.00866

1

2 Table presents the characteristics of these models. Therefore, by comparing models 1 and 6, it is  
3 possible to see the effect of beam and displacement change on wave height and by comparing models  
4 2 and 6, make it possible to see the effect of altering beam and draught, but maintaining displacement.  
5 The simulations were conducted in a channel with 3.5m width and 1.5m depth. Figure to Figure  
6 illustrate the results for the aforementioned models at different  $Fr_h$ .

7 The results show that by increasing the model beam, the generated wave height increases for all  
8 investigated  $Fr_h$ . The wave height of model 6 which has greater beam (the width of model 6 is about  
9 44% larger than models 1 and 2) is about 28% to 98% larger than wave height for models 1 and 2 at  
10 various lateral distances. The comparison between models 1, 2 and 6 shows that adding displacement  
11 increases wave height, however the increase by increasing draught is small, whereas the increase due  
12 to a beam increase is large. The difference between models 6 and 2 can be explained by considering  
13 that the waterplane of Model 6 is larger than Model 2 (

	Draught (m)	Beam (m)	LWL (m)	Water plane (m <sup>2</sup> )	Angle of attack (degree)	Volume displacement (m <sup>3</sup> )
Model 1	0.1	0.3	0.40	0.120	14	0.006
Model 2	0.12	0.3	0.48	0.144	14	0.00866
Model 6	0.1	0.433	0.40	0.174	14	0.00866

14

15 Table ). Therefore increasing the displacement by increasing the beam generates a higher wave than  
16 increasing the draught. It is predicted that increasing the beam will increase the wave height till wave  
17 starts to break and then further increase of beam does not have influence on the wave height.

### 18 Pressure source profile shape

19 According to the angle of attack study results, it was seen that the waves generated by a 4 degree  
20 angle of attack model had almost constant height across the channel while the model with angle of  
21 attack of 14 degrees generated higher waves. However, the bow waves generated by the 4 degree  
22 angle of attack were larger than those of the 14 degree angle of attack. A new model (model 8) was

1 generated. This model has a constant beam, with a 14 degree angle of attack at the front and a 4  
 2 degree angle of attack at the stern (

<b>Beam (m)</b>	0.3
<b>Length of water line (m)</b>	0.4
<b>Angle of attack in front (degree)</b>	14
<b>Angle of attack in stern (degree)</b>	4
<b>Draught (m)</b>	0.1

3  
 4 Table ). Figure shows model 8 schematically. Figure to Figure show the results between model 1  
 5 (14 degree angle of attack), model 5 (4 degree angle of attack) and model 8. The wave generated  
 6 heights for model 8 are smaller than those of model 1, but the wave height decrease of between  
 7  $y^*=0.57$  and  $y^*=0.71$  lateral distances is slightly less compared to model 1.

8 According to the results, it can be concluded that the angle of attack in front of model (at the  
 9 stagnation point) is more effective in wave generated height. While the angle of attack at transom can  
 10 has effect on wave quality. It means, the wave height decrease of between 1.0 m and 1.25 m lateral  
 11 distances is slightly less compared to model 1 and more than model 8.

## 12 Channel parameters

### 13 Depth

14 The effect of water depth on generated wave height was investigated. Three water depths were  
 15 considered and the wanedozer with 0.1 m draught and 0.3 m beam was simulated at three different  
 16 speeds. The only difference between channels was the water depth.

	V [m/s]			
	<i>h</i> [m]	1.66	1.99	2.66
<b>Channel 1</b>	0.4	0.838	1	1.343
<b>Channel 2</b>	0.45	0.79	0.947	1.266
<b>Channel 3</b>	0.5	0.75	0.9	1.2

17  
 18 Table presents  $Fr_h$  for the given speeds at different water depths.  $Fr_h$  values at 1.66 m/s forward  
 19 speed for all three different depths are less than 1 (sub-critical  $Fr_h$ ). Figure shows the wave height  
 20 results at 1.66 m/s speed for the three different water depths. According to the results, the generated  
 21 wave in the shallowest water has the largest wave height, because it has the highest  $Fr_h$ .

22 The  $Fr_h$  at 1.99 m/s speed and 0.4 m water depth is equal to 1. The simulation results show the  
 23 generated bow wave (soliton wave) at this condition is larger than for the two other conditions and the



1 wave behind the pressure source has the lowest height at  $Fr_h=1.0$  (Figure ). Figure presents the wave  
 2 heights at different lateral distances for three different water depths at 1.99 m/s speed. Figure presents  
 3 the results for 2.66 m/s at different water depths. The  $Fr_h$  for all three conditions are larger than 1.  
 4 Figure shows the time history of surface elevation at 0.75 lateral distances for 2.6 m/s speed at three  
 5 different water depths. It can be seen that the shape of the waves are the same for  $Fr_h$  larger than 1.2.  
 6 It means the water depth does not have influence on the wave shape. Because the  $Fr_h$  values are  
 7 greater than one, the downstream pressure does not have an effect on the up-stream.

### 8 **Blockage factor**

9 By changing the water depth, depth Froude number and blockage factor will change simultaneously.  
 10 It was shown in the previous section that changing the water depth has an effect on the generated  
 11 wave characteristics. To separate the effect of depth Froude number and blockage factor by changing  
 12 the water depth, a new channel was modelled (channel 4) and the results were compared with the two  
 13 other channels results.

	<b>Width (m)</b>	<b>Depth (m)</b>	<b>Blockage factor (<math>\kappa</math>)</b>
<b>Channel 1</b>	3.5	0.4	0.0214
<b>Channel 3</b>	3.5	0.5	0.0171
<b>Channel 4</b>	4.375	0.4	0.0171

14  
 15 Table presents the parameters of the three channels which were used for this comparison. Channels 1  
 16 and 4 have the same water depth, and channels 3 and 4 have the same blockage factor but different  
 17 water depths. The results for the three different speeds 1.66, 1.99 and 2.66 m/s are presented in Figure  
 18 to Figure .

19 The results indicate that the effect of depth Froude number on wave height is more important than the  
 20 blockage factor for  $Fr_h < 1.0$  and the blockage factor at this range of  $Fr_h$  is negligible. Therefore,  
 21 higher  $Fr_h$  generates larger wave (Figure 34). In Figure 35, model in Channel 3 is in sub-critical  
 22 ( $Fr_h=0.9$ ) and model in Channels 1 and 4 are in critical ( $Fr_h=1.0$ ) Froude depth values. At  
 23 supercritical Froude depth values the channel with lowest blockage factor generates the highest wave  
 24 (Figure 36). More investigations are required to find the highest ineffective blockage factor. At  
 25 highest ineffective blockage factor the channel cross section would be smallest cross section which  
 26 does not have influence on the wave generated parameters.

## 1 **Concluding remarks**

2 In this study the influence of pressure source parameters, depth and blockage factors were  
3 investigated. Draught, angle of attack, beam and profile shape were investigated as the effective  
4 parameters of pressure source on wave height. Since the first wave behind the pressure source was  
5 considered as surfable wave, the effect of parameters on this wave was investigated.

6 The investigation indicated that increasing draught, angle of attack and beam will increase the wave  
7 height generated, while it was shown that wave height variation across the channel for a lower angle  
8 of attack is less than others. The pressure gradient will increase by increasing the angle of attack.  
9 Hence the wave generated by higher angle of attack wadedozer is larger than the lower. Comparing  
10 the results for the two different wadedozers with the same displacement and angle of attack, but  
11 different beam and draught, it can be seen that the model with the wider beam generates a higher  
12 wave. This means that the effect of beam on generated waves is greater than the effect of draught. The  
13 model with larger beam has larger water plane which means the volume of displacement close to free  
14 surface for model with larger beam is bigger than the model with larger draught. Consequently, the  
15 wave generated by wider wadedozer is higher than other one. Meanwhile, it is expected that there is  
16 limitation for effective draught and the draught larger than that does not have effect on wave  
17 generated height. Since only the portion of displacement close to free surface has effect on the wave  
18 generated. Increasing the beam with increase the wave height till the wave generated does not break.

19 The water depth study showed that by decreasing the water depth for a given speed, larger wave  
20 height will be generated as long as the  $Fr_h$  is subcritical. When  $Fr_h=1$  the bow (soliton) wave  
21 generated is higher than the wave behind the pressure source. It was also shown that water depth does  
22 not have an effect on the wave height for  $Fr_h$  more than 1.2. It means for this range of  $Fr_h$  the  
23 downstream does not have influence on upstream, because the pressure source moves faster than wave  
24 speed.

25 The blockage factor was investigated. The results indicate that the effect of depth Froude number on  
26 wave height is more important than the blockage factor for subcritical Froude depth values and the  
27 blockage factor at this range is negligible. At supercritical Froude depth values the channel with  
28 lowest blockage factor generates the highest wave. Further simulations are needed to find the highest  
29 ineffective blockage factor.

## 30 **Acknowledgement**

31 The authors thank the Australian Research Council (ARC), University of Tasmania, and Liquid Time  
32 Pty Ltd., which funded this research. This research was supported under the ARC Linkage Projects  
33 funding scheme (Project LP0990307).

## 1 References

- 2 [1] Georgiadis, C. "Modeling Boat Wake Loading on Long Floating Structures," *Computers &*  
3 *Structures*, vol. 18, no. 4, pp. 6 (1984).
- 4 [2] Dam, K. T., Tanimoto, K., Nguyen, B. T. and Akagawa, Y. "Numerical Study of Propagation  
5 of Ship Waves on a Sloping Coast," *Ocean Engineering*, vol. 33, pp. 15 (2006).
- 6 [3] Jiankang, W., Lee, T. S. and Shu, C. "Numerical Study of Wave Interaction Generated by  
7 Two Ships Moving Parallely in Shallow Water," *Computer Methods in Applied Mechanics*  
8 *and Engineering*, vol. 190, pp. 12 (2001).
- 9 [4] Nanson, G., Krusenstierna, A. V., Bryant, E. and Renilson, M. "Experimental Measurements  
10 of River Bank Erosion Caused by Boat-Generated Waves on the Gordon River, Tasmania,"  
11 *Regulated Rivers, Research and Management*, vol. 9, pp. 14 (1994).
- 12 [5] Renilson, M. R. and Lenz, S. "An Investigation into the Effect of Hull Form on the Wake  
13 Wave Generated by Low Speed Vessels.", *22nd American Towing Tank Conference*, p. 6  
14 (1989).
- 15 [6] Robbins, A., Thomas, G., Renilson, M. and Macfarlane, G. "Subcritical Wave Wake  
16 Unsteadiness," *RINA Transactions, International Journal of Maritime Engineering*, vol. 153,  
17 Part A3 (2011).
- 18 [7] Zibell, H. G., and Grollius, W. "Fast vessels on inland waterways.", in *The RINA*  
19 *International Conference on Coastal Ships and Inland Waterways*, London, England (1999).
- 20 [8] Macfarlane, G. J. and Bose, N. "Wave Wake: Focus On Vessel Operations Within Sheltered  
21 Aterways," *SNAME*, vol. 006 (2012).
- 22 [9] Koushan, K., Werenskiold, P. and Zhao, R. "Experimental And Theoretical Investigation Of  
23 Wake Wash," in *FAST*, Southampton, UK, pp. 165-179 (2001).
- 24 [10] Chandraprabha, S. and Molland, A. F. "A Numerical Preiction Of Wash Wave And Wave  
25 Resistance Of High Speed Displacement Ships In Deep And Shallow Water," in *Conference*  
26 *Of Mechanical Engineering Network Of Thailand*, Khon Kaen, Thailand (2004).
- 27 [11] Fontaine, E. and Tulin, M. P. "On The Prediction Of Nonlinear Free-Surface Flows Past  
28 Slender Hulls Using 2D+T Theory: The Evolution Of An Idea," in *Fluid Dynamics Of*  
29 *Vehicles Operating Near Or In The Air-Sea Interface*, Amsterdam, Netherland (1998).
- 30 [12] Henn, R., Sharma, S. D. and Jiang, T. "Influence Of Canal Topography On Ship Waves In  
31 Shallow Water," in *16th International Workshop On Water Waves And Floating Bodies*,  
32 Hiroshima, Japan (2001).
- 33 [13] Yang, Q., Faltinsen, O. M. and Zhao, R. "Wash Of Ships In Finite Water Depth," in *FAST*,  
34 Southampton, UK, pp. 181-196 (2001).
- 35 [14] Raven, H. C. "Numerical Wash Prediction Using A Free-Surface Panel Code," in  
36 *International Conference on Hydrodynamics of High-Speed Craft - Wake Wash and Motion*  
37 *Control*, London, UK (2000).
- 38 [15] Kofoed-Hansen, H., Jensen, T. and Sørensen, O. R. "Wake Wash Risk Assessment Of High-  
39 Speed Ferry Routes – A Case Study And Suggestions For Model Improvements," in  
40 *International Conference on Hydrodynamics of High-Speed Craft - Wake Wash and Motion*  
41 *Control*, London, UK (2000).
- 42 [16] Kim, Y. "Artificial Damping In Water Wave Problems II: Application to Wave Absorption,"  
43 *International Journal of Offshore and Polar Engineering*, vol. 13, pp. 5 (2003).
- 44 [17] Javanmardi, M., Binns, J., Renilson, M. R., Thomas, G. and Huijsmans, R. "The Formation  
45 Of Surfable Waves In A Circular Wave Pool- Comparison Of Numerical And Experimental  
46 Approaches," in *31th International Conference on Ocean, Offshore and Arctic Engineering*,  
47 Rio de Janeiro, Brazil (2012).
- 48 [18] Javanmardi, M., Binns, J., Thomas, G. and Renilson, M. R. "Prediction Of Water Wave  
49 Propagation Using Computational Fluid Dynamics." in *32th International Conference on*  
50 *Ocean, Offshore and Arctic Engineering*, Nantes, France (2013).
- 51 [19] Driscoll, A., and Renilson, M. R. "The wavedozer. A system of generating stationary waves  
52 in a circulating water channel," *AMTE(H) TM80013* (1980).
- 53 [20] "ANSYS FLUENT User's Guid," ANSYS, Inc. (2011).

1

2 **Mohammadreza Javanmardi** is Adjunct Assistant Professor at Sharif University of Technology. His  
3 research focusses on the ship hydrodynamics, maneuvering, wave, Computational Fluid Dynamics and  
4 experimental tests.

5

6 A/ Professor Jonathan Richard Binns, Associate Dean Research, Australian Maritime College; Director,  
7 ARC Research Training Centre for Naval Design and Manufacturing, University of Tasmania. Jonathan  
8 Binns has trained and worked as a design and research engineer specialising in analysis of fluid  
9 mechanics by theoretical and experimental means. His primary expertise is in a variety of model and  
10 full scale experiments as well as potential flow and finite volume flow predictions. Jonathan has  
11 experience in hydrodynamic and structural design, research, development and simulation of marine  
12 craft.

13

14 Martin Renilson is an Adjunct Professor in Hydrodynamics at the University of Tasmania. His previous  
15 experience includes as Technical Manager and Deputy General Manager for the Maritime Platforms  
16 and Equipment Group at QinetiQ.

17

18 Giles Thomas is BMT Chair of Maritime Engineering in University College London's Department of  
19 Mechanical Engineering. A naval architect, his research focusses on the performance of ships, boats  
20 and offshore structures. Specific interests include fluid-structure interaction, hydrodynamics, full scale  
21 measurements, model testing and design. He is a Fellow of the Royal Institution of Naval Architects  
22 (RINA) and a Chartered Engineer (CEng – Engineering Council of Great Britain).

23

24

## 1 **Figure captions**

- 2 Figure 1. Wavedozer model attached to the towing Tank carriage.
- 3 Figure 2. Layout of probes with pressure source.
- 4 Figure 3. Computational grid domain.
- 5 Figure 4. Comparison of experiment and numerical drag coefficients for different  $Fr_h$  at 1500mm
- 6 water depth.
- 7 Figure 5. Comparison of experiment and numerical lift coefficients for different  $Fr_h$  at 1500mm water
- 8 depth.
- 9 Figure 6. Free-surface elevation for  $Fr_h=0.7$  at 750mm lateral distance from centre-line (WP1).
- 10 Figure 7. Free-surface elevation for  $Fr_h=0.99$  at 750mm lateral distance from centre-line (WP1).
- 11 Figure 7. Free-surface elevation for  $Fr_h=0.99$  at 1000mm lateral distance from centre-line (WP2).
- 12 Figure 8. Free-surface elevation for  $Fr_h=0.99$  at 1250mm lateral distance from centre-line (WP3).
- 13 Figure 9. Non-dimensional wave heights variation with respect to lateral distances for model 1 and
- 14 model 2 at  $Fr_h=0.75$ .
- 15 Figure 10. Non-dimensional wave heights variation with respect to lateral distances for model 1 and
- 16 model 2 at  $Fr_h=0.9$ .
- 17 Figure 12. Non-dimensional wave heights variation with respect to lateral distances for model 1 and
- 18 model 2 at  $Fr_h=0.95$ .
- 19 Figure 13. Non-dimensional wave heights variation with respect to lateral distances for model 1 and
- 20 model 2 at  $Fr_h=0.99$ .
- 21 Figure 11. Wave height generated variation with respect to angle of attack (AoA) at different lateral
- 22 distances for  $Fr_h=0.75$ .
- 23 Figure 12. Wave height generated variation with respect to angle of attack (AoA) at different lateral
- 24 distances for  $Fr_h=0.9$ .
- 25 Figure 13. Wave height generated variation with respect to angle of attack (AoA) at different lateral
- 26 distances for  $Fr_h=0.95$ .
- 27 Figure 14. Wave height generated variation with respect to angle of attack (AoA) at different lateral
- 28 distances for  $Fr_h=0.99$ .
- 29 Figure 15. The drag coefficients variation with respect to Angle of Attack at different  $Fr_h$ .
- 30 Figure 16. The lift coefficients variation with respect to Angle of Attack at different  $Fr_h$ .

1 Figure 17. Non-dimensional wave heights variation with respect to lateral distances for models 1, 2  
2 and 6 at  $Fr_h=0.75$ .

3 Figure 18. Non-dimensional wave heights variation with respect to lateral distances for models 1, 2  
4 and 6 at  $Fr_h=0.9$ .

5 Figure 19. Non-dimensional wave heights variation with respect to lateral distances for models 1, 2  
6 and 6 at  $Fr_h=0.95$ .

7 Figure 20. Non-dimensional wave heights variation with respect to lateral distances for models 1, 2  
8 and 6 at  $Fr_h=0.99$ .

9 Figure 21. Model 8 of  $B=0.3\text{m}$ ,  $LWL=0.4\text{m}$ ,  $AOA$  at transom= $4$  degrees,  $AOA$  at front= $14$  degrees  
10 and  $D=0.1\text{m}$ .

11 Figure 22. Non-dimensional wave heights variation with respect to lateral distances for model 1, 5 and  
12 8 for  $Fr_h=0.75$ .

13 Figure 23. Non-dimensional wave heights variation with respect to lateral distances for model 1, 5 and  
14 8 for  $Fr_h=0.9$ .

15 Figure 24. Non-dimensional wave heights variation with respect to lateral distances for model 1, 5 and  
16 8 for  $Fr_h=0.95$ .

17 Figure 25. Non-dimensional wave heights variation with respect to lateral distances for model 1, 5 and  
18 8 for  $Fr_h=0.99$ .

19 Figure 26. Non-dimensional wave heights variation with respect to lateral distances for three different  
20 water depths at  $1.66\text{ m/s}$  speed.

21 Figure 27. Free-surface elevation at  $0.75\text{ m}$  lateral distances at  $1.99\text{ m/s}$  speed for three different water  
22 depths.

23 Figure 28. Non-dimensional wave heights variation with respect to lateral distances for three different  
24 water depths at  $1.99\text{ m/s}$  speed.

25 Figure 29. Non-dimensional wave heights variation with respect to lateral distances for three different  
26 water depths at  $2.66\text{ m/s}$  speed.

27 Figure 30. Free-surface elevation at  $0.75\text{ m}$  lateral distances at  $2.66\text{ m/s}$  speed for three different water  
28 depths.

29 Figure 31. Wave heights variation with respect to lateral distances for three different water depths at  
30  $1.66\text{ m/s}$  speed.

31 Figure 32. Wave heights variation with respect to lateral distances for three different water depths at  
32  $1.99\text{ m/s}$  speed.

1 Figure 33. Wave heights variation with respect to lateral distances for three different water depths at  
2 2.66 m/s speed.

### 3 **Table captions**

4 Table 1. Wavedozer Principal Particulars.

5 Table 2. Wavedozers dimensions.

6 Table 3. Wavedozers with different angle of attack parameters.

7 Table 4. The pressure sources characteristics.

8 Table 5. The characteristics of model 8.

9 Table 6.  $Fr_h$  for different speeds at different water depth.

10 Table 7. Three different channels parameters for blockage factor investigation.

11

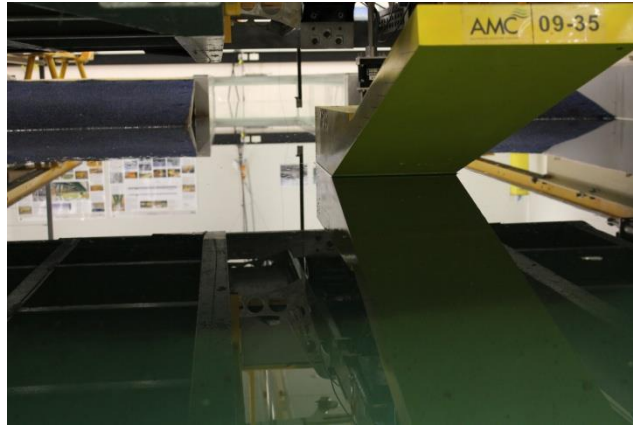


Figure 1.

Length (m)	1.5
Beam (m)	0.3
Draft(m)	0.1
Angle of attack (deg.)	14

Table 1.

1  
2

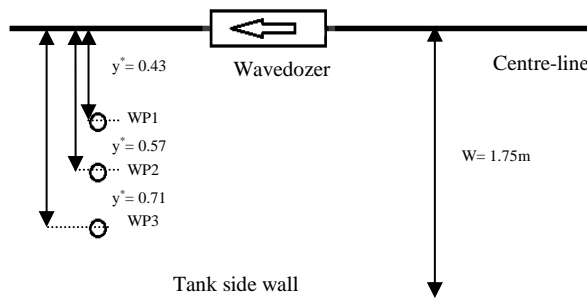


Figure 2.

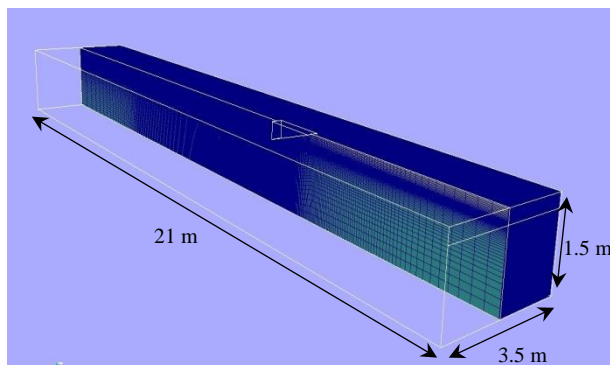


Figure 34.



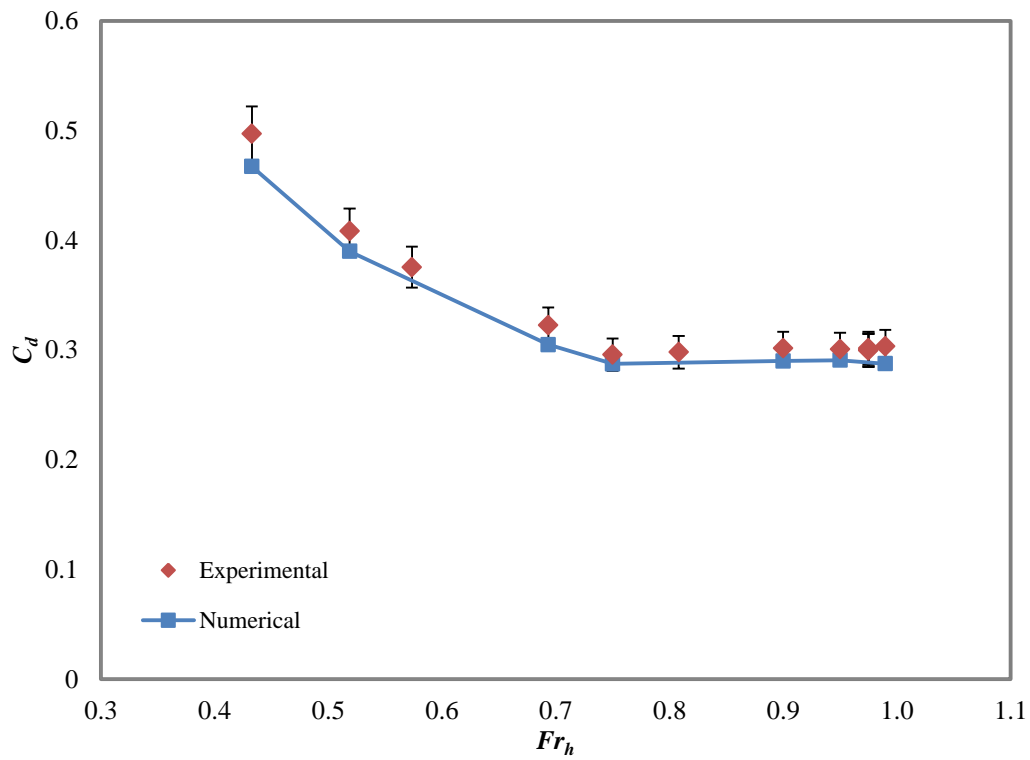


Figure 4.

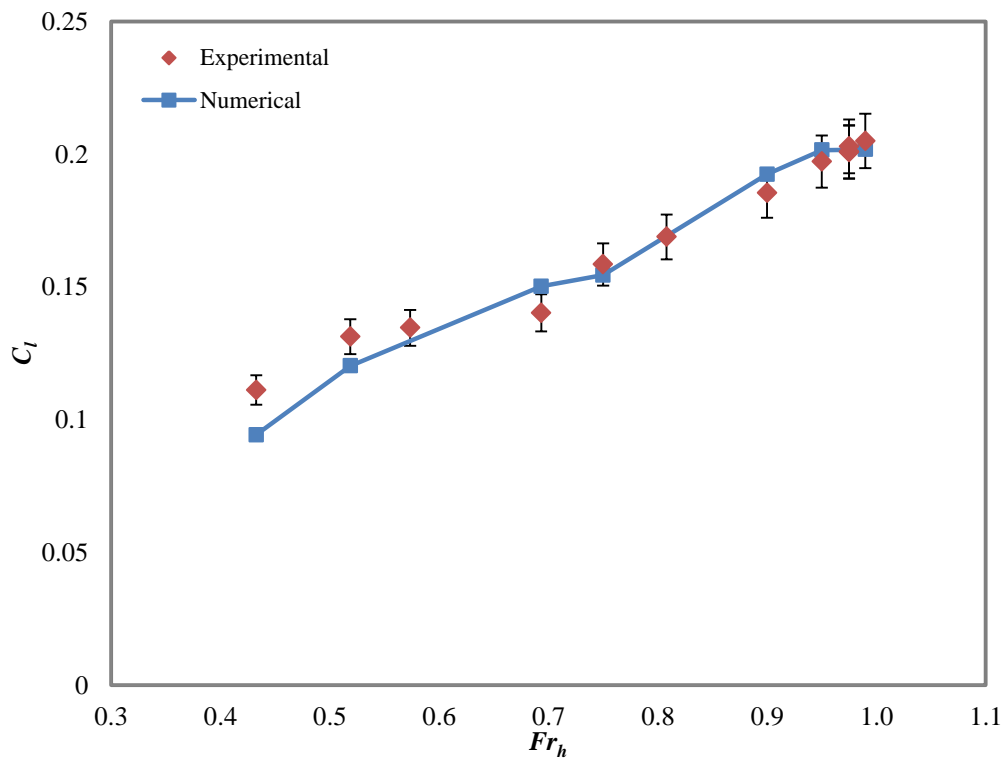


Figure 5.

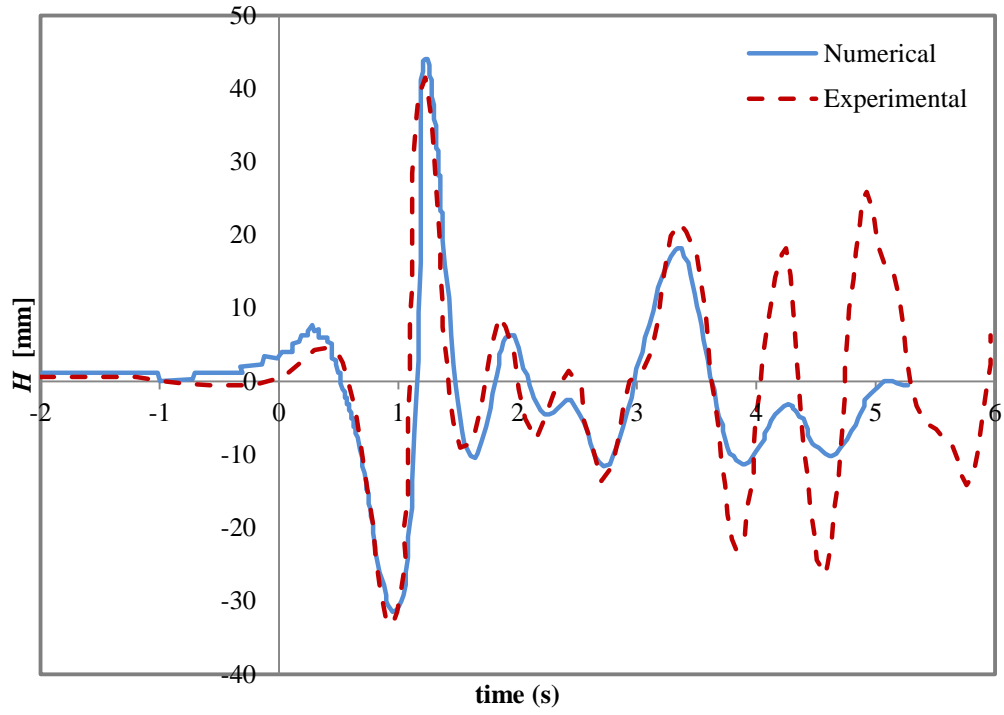


Figure 6.

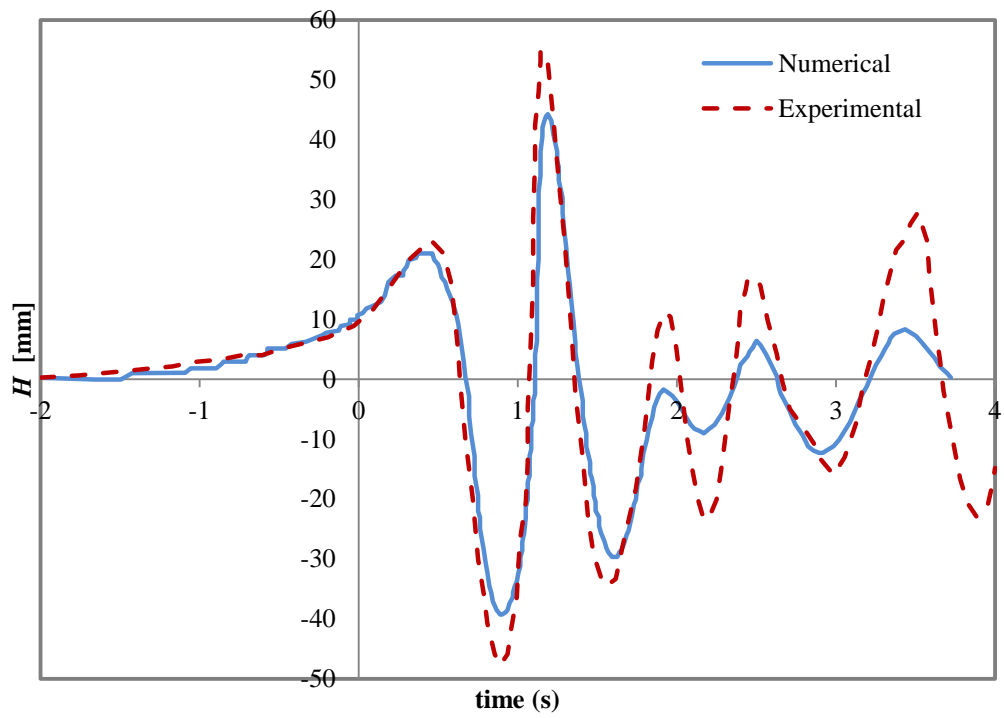


Figure 7.

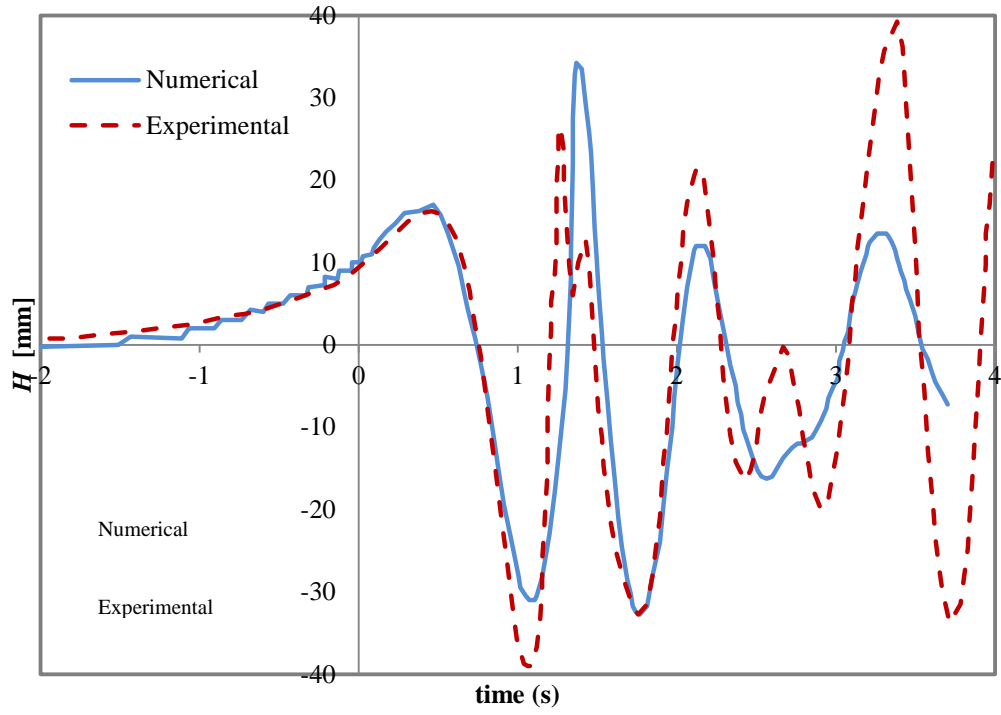


Figure 8.

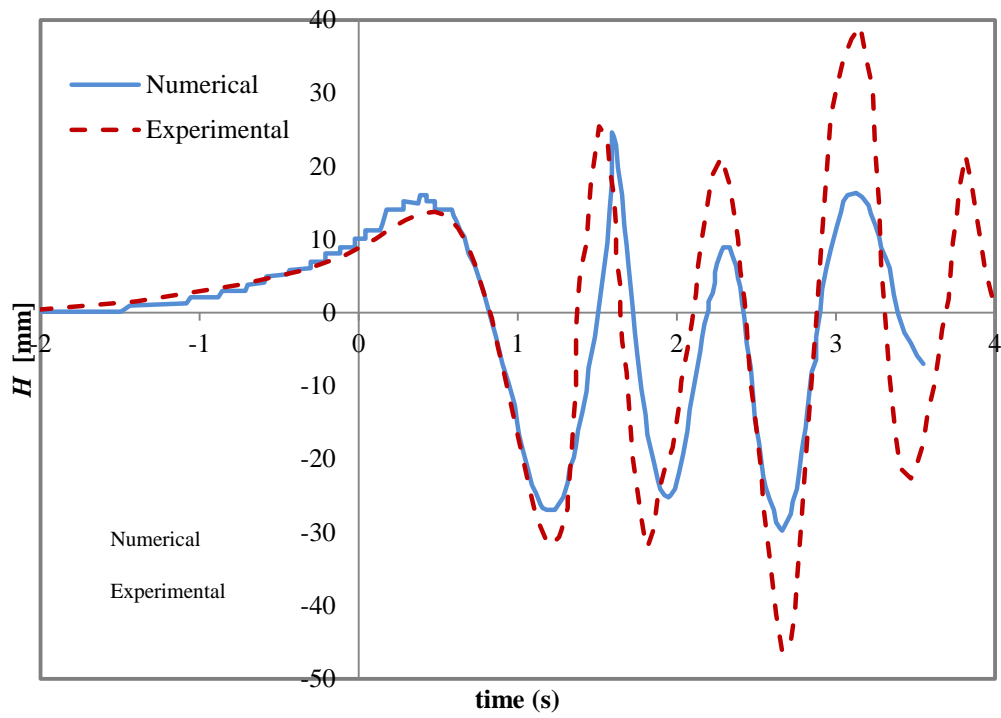


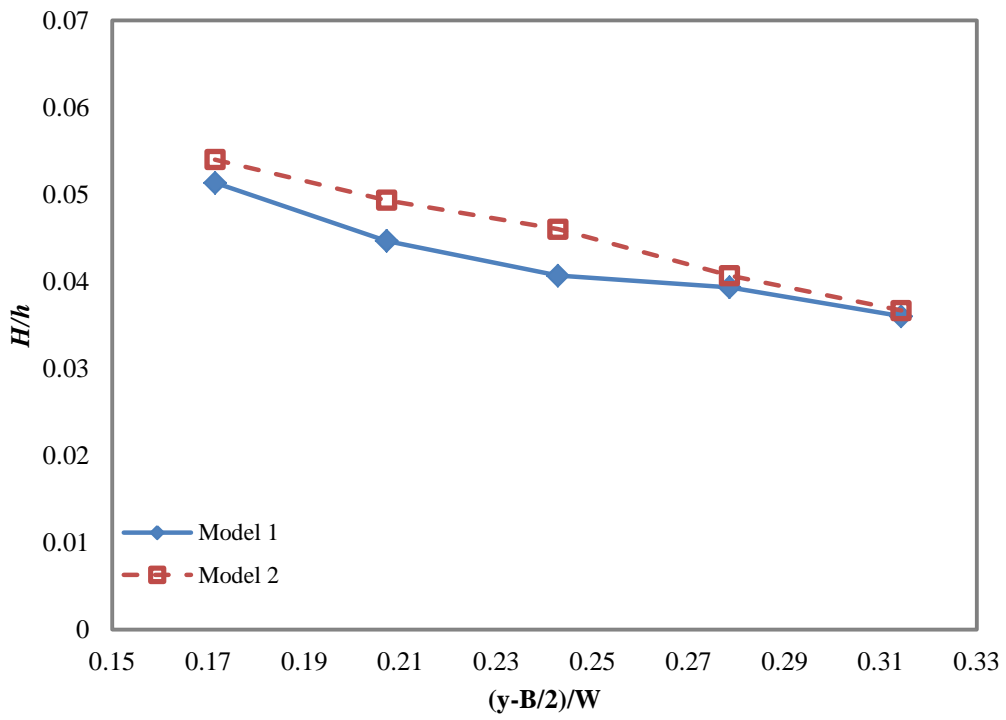
Figure 9.

- 1
- 2
- 3

	<b>Draught (m)</b>	<b>Beam (m)</b>	<b>Angle of attack (deg)</b>	<b>LWL (m)</b>	<b>Displacement (m<sup>3</sup>)</b>	<b>Blockage factor</b>
<b>Model 1</b>	0.1	0.3	14	0.40	0.006015	0.0057
<b>Model 2</b>	0.12	0.3	14	0.48	0.00866	0.0068

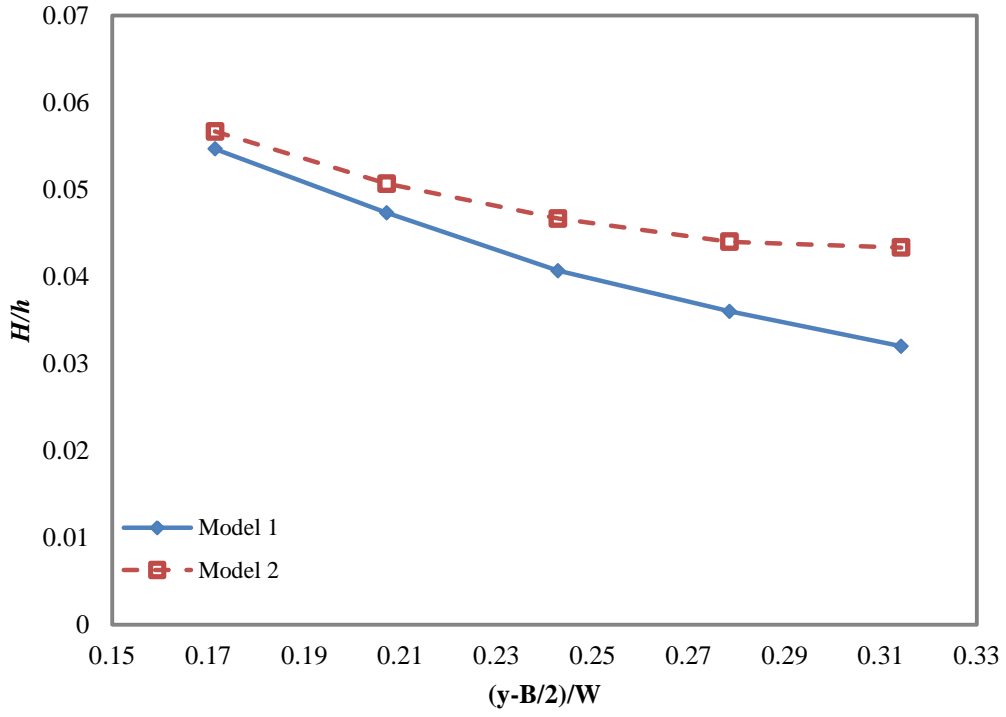
1  
2  
3

**Table 2.**



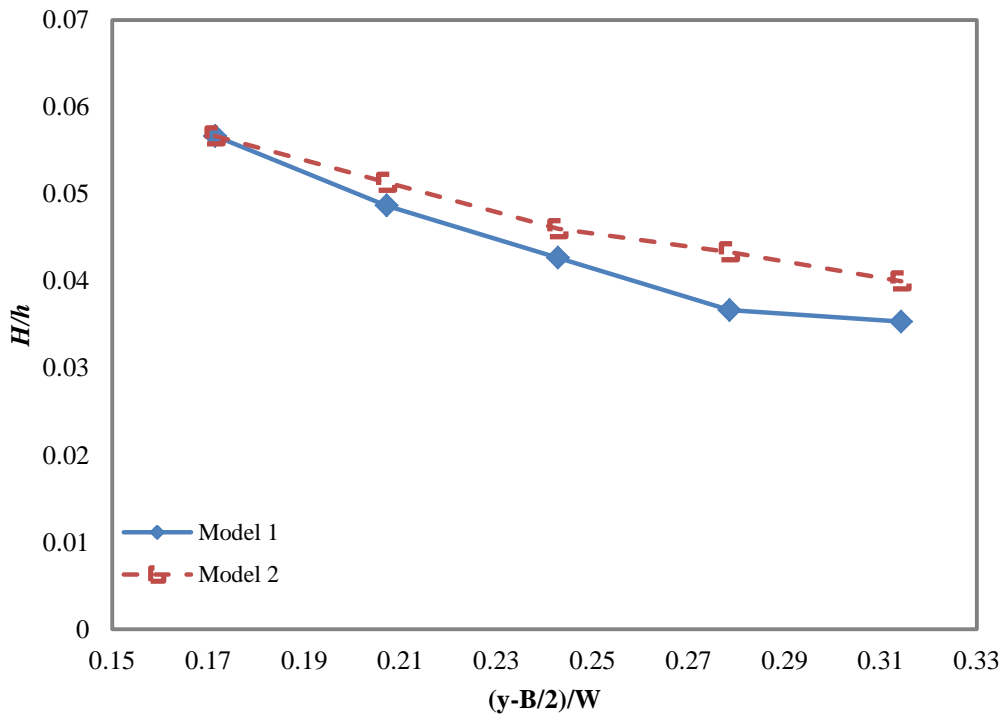
4  
5

**Figure 10.**



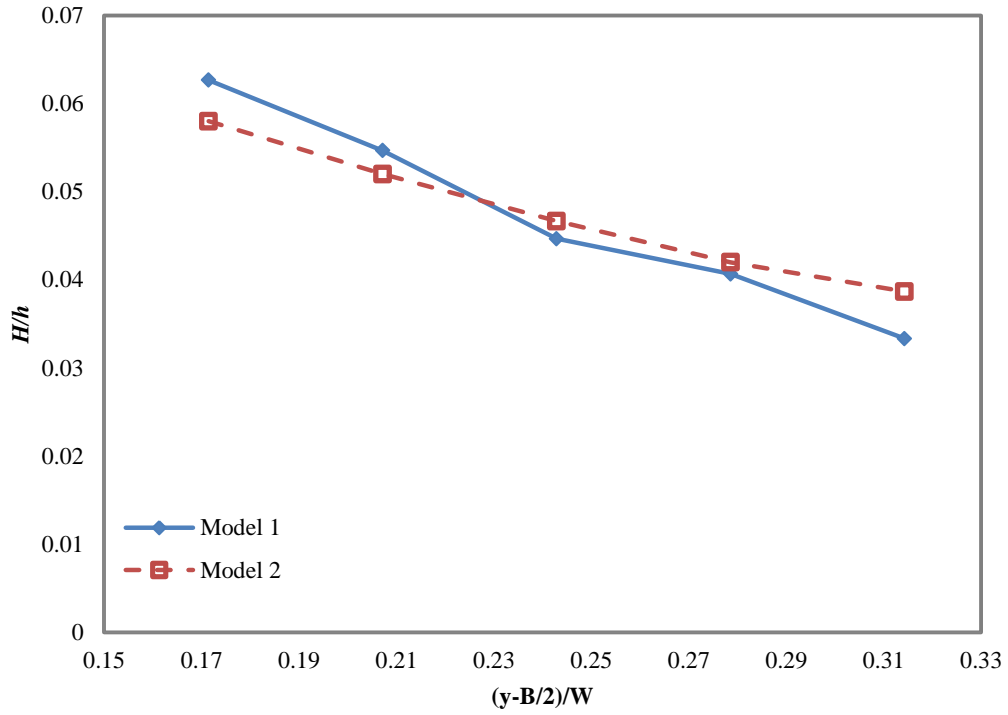
1  
2

Figure 11.



3  
4

Figure 12.



1

2

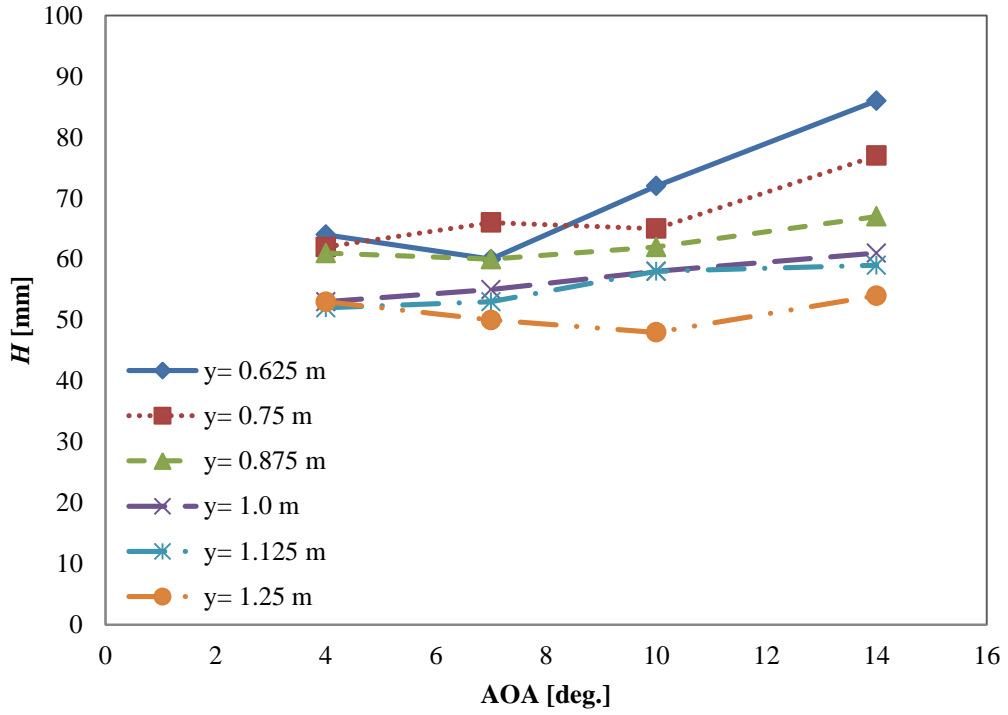
Figure 13.

	<b>Draught (m)</b>	<b>Beam (m)</b>	<b>Angle of attack (deg.)</b>	<b>LWL (m)</b>	<b>Displacement (m<sup>3</sup>)</b>	<b>Blockage factor</b>
<b>Model 1</b>	0.1	0.3	14	0.401	0.006015	0.0057
<b>Model 3</b>	0.1	0.3	10	0.567	0.008505	0.0057
<b>Model 4</b>	0.1	0.3	7	0.814	0.01221	0.0057
<b>Model 5</b>	0.1	0.3	4	1.43	0.02145	0.0057

3

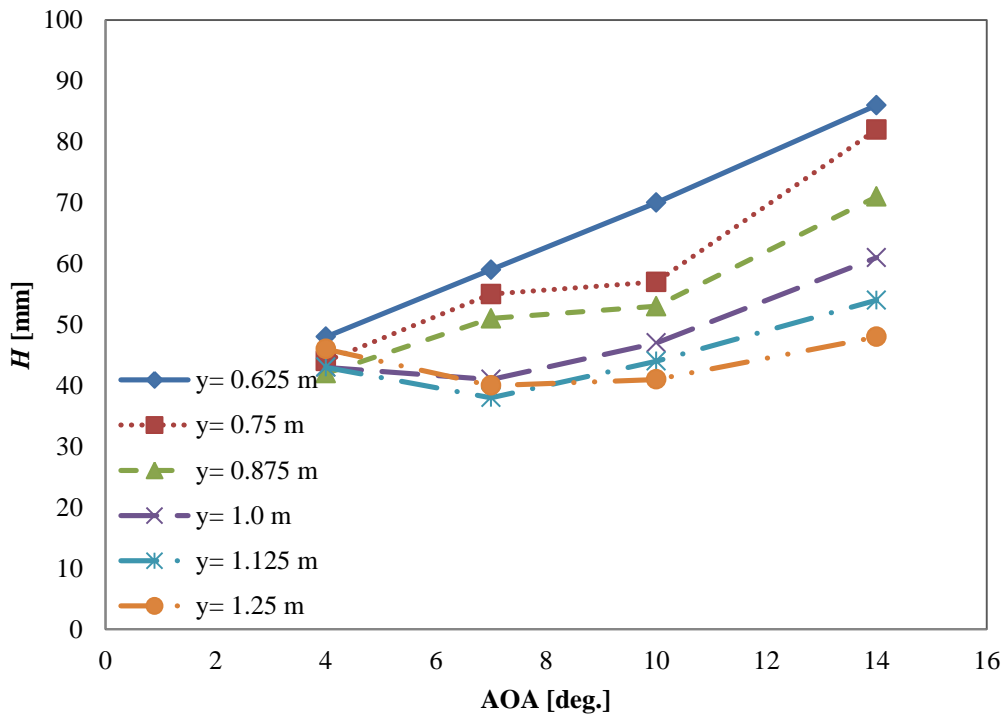
4

Table 3.



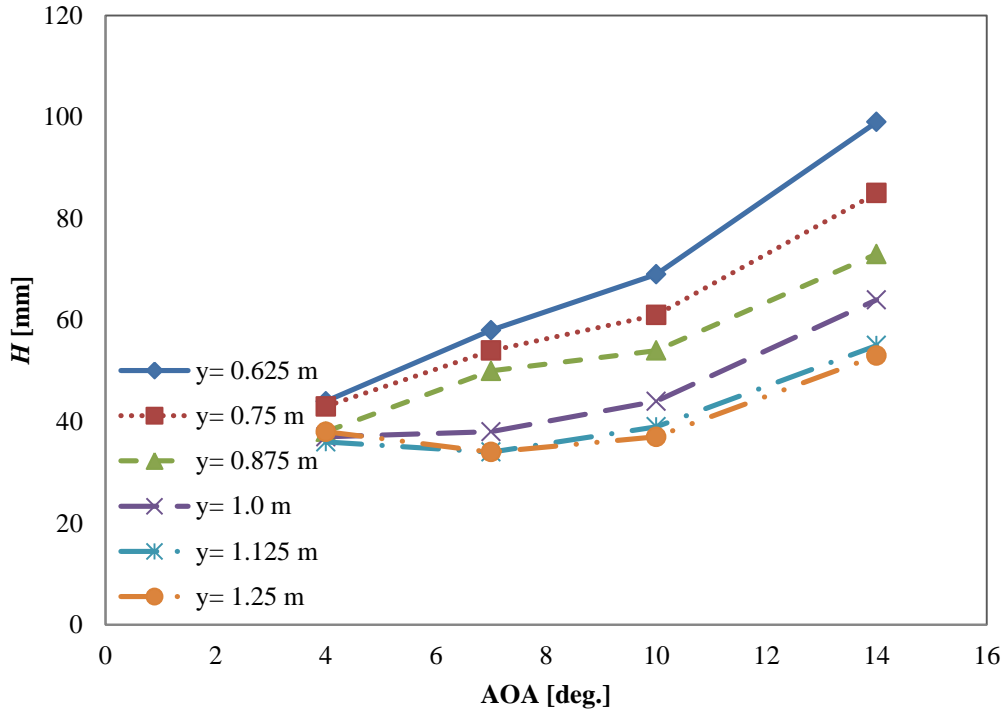
1  
2

Figure 14.



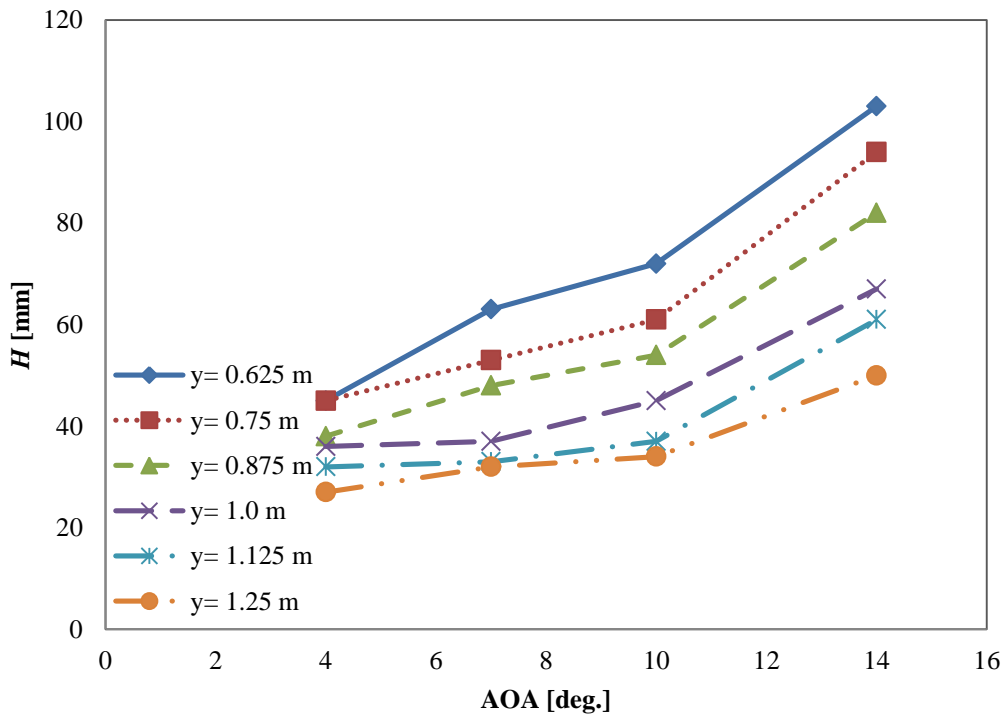
3  
4  
5

Figure 15.



1  
2

Figure 16.



3  
4  
5  
6

Figure 17.



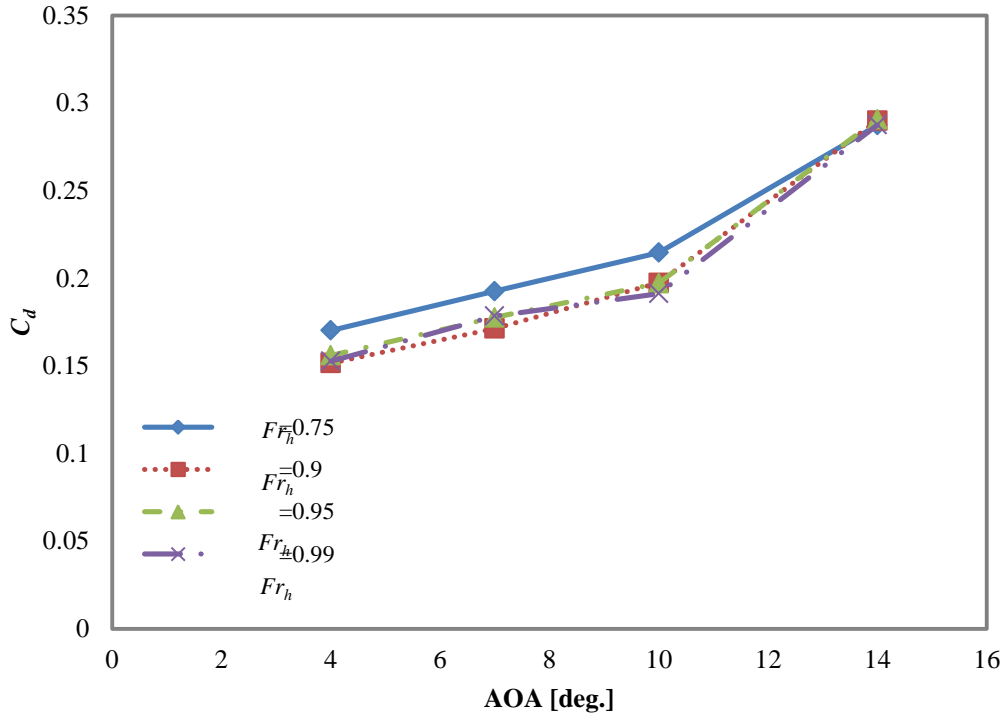


Figure 18.

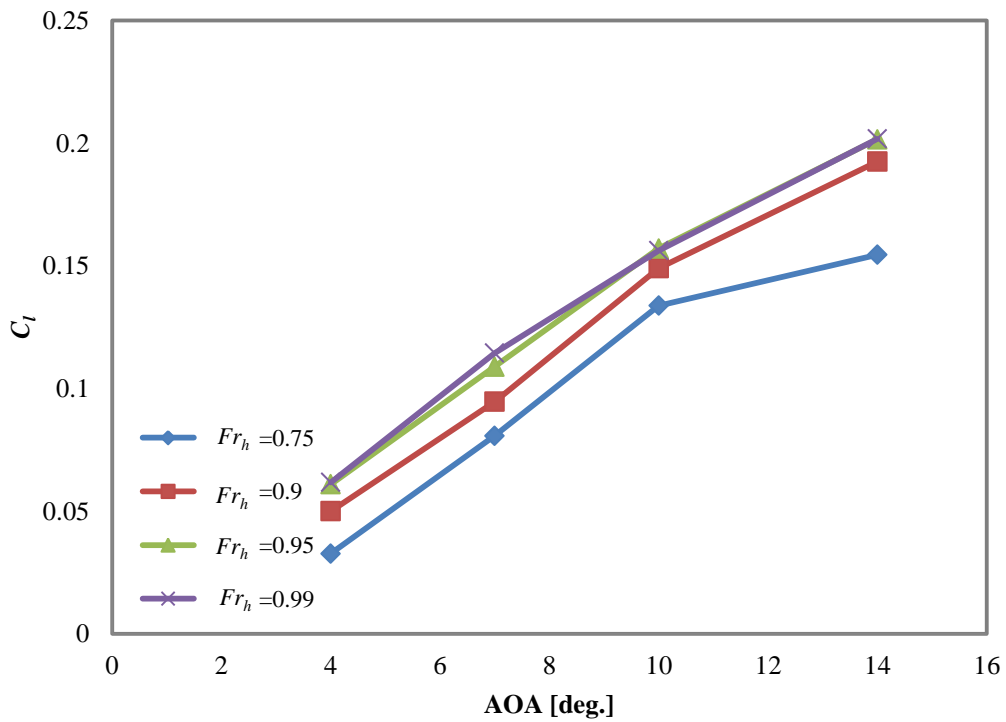


Figure 19.

	Draught	Beam	LWL	Water plane	Angle of attack	Volume displacement
--	---------	------	-----	-------------	-----------------	---------------------

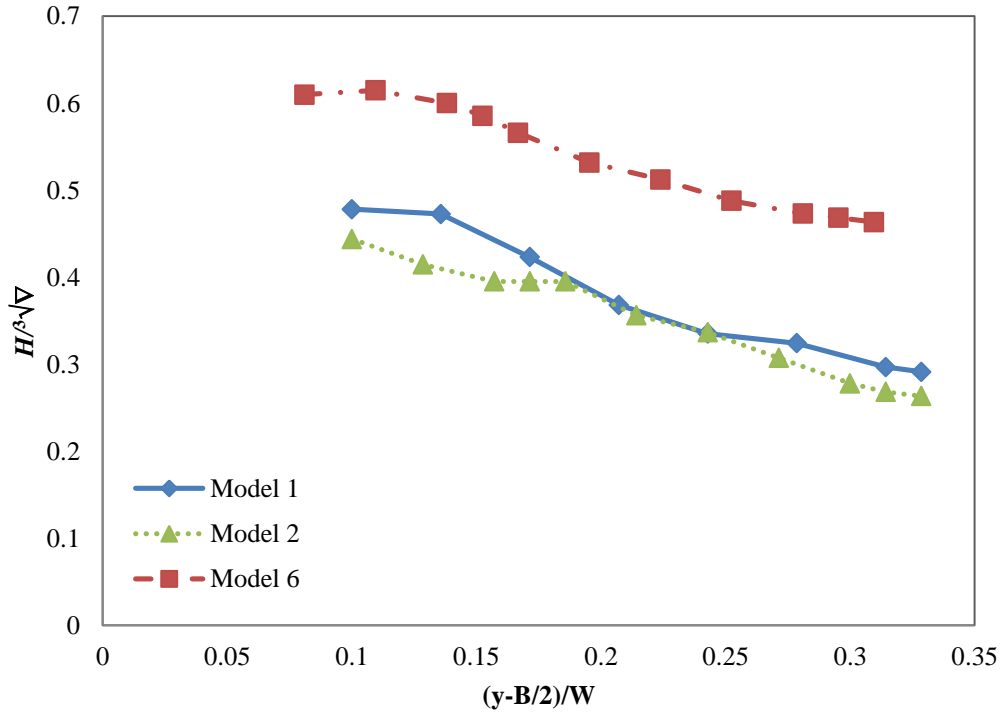
1  
2  
3

4  
5

	(m)	(m)	(m)	(m <sup>2</sup> )	(degree)	(m <sup>3</sup> )
Model 1	0.1	0.3	0.40	0.120	14	0.006
Model 2	0.12	0.3	0.48	0.144	14	0.00866
Model 6	0.1	0.433	0.40	0.174	14	0.00866

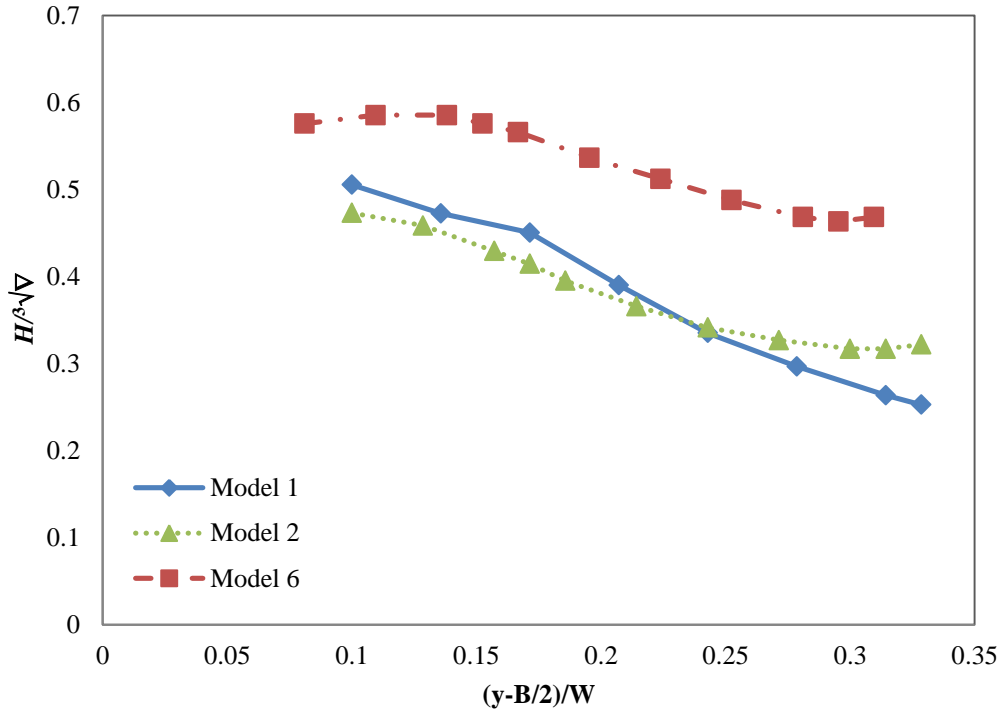
1  
2

**Table 4.**



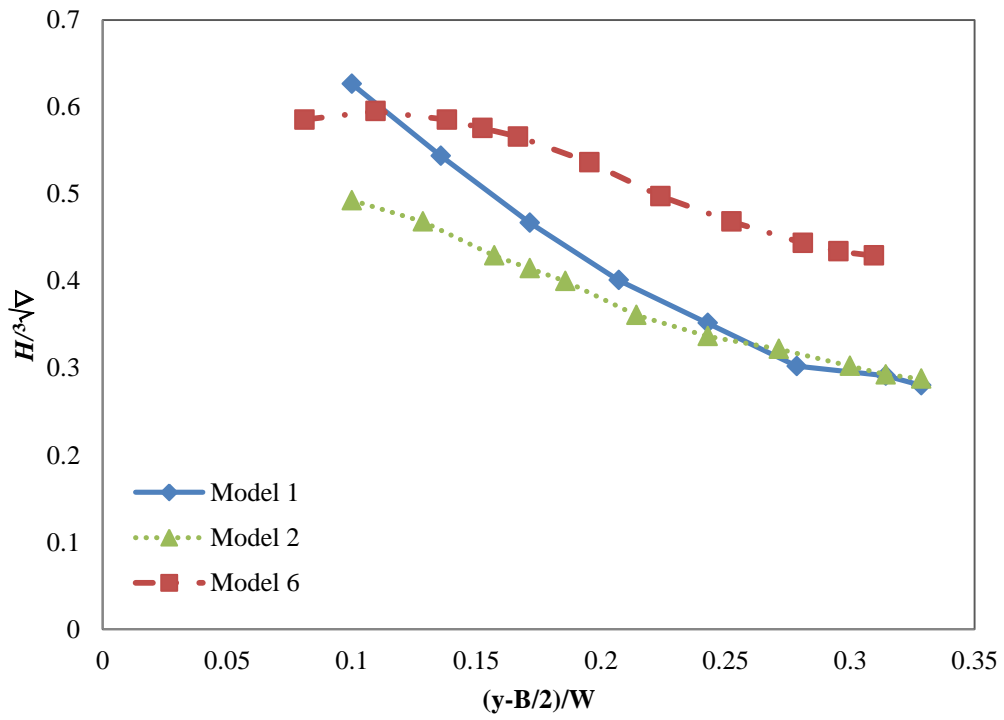
3  
4

**Figure 20.**



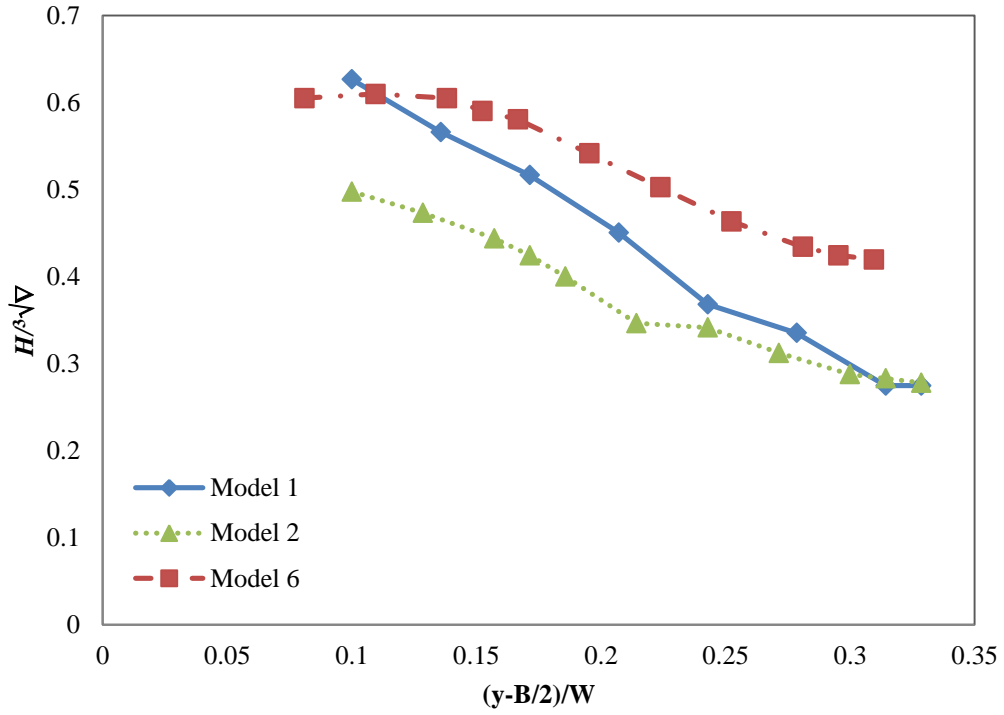
1  
2

Figure 21.



3  
4

Figure 22.



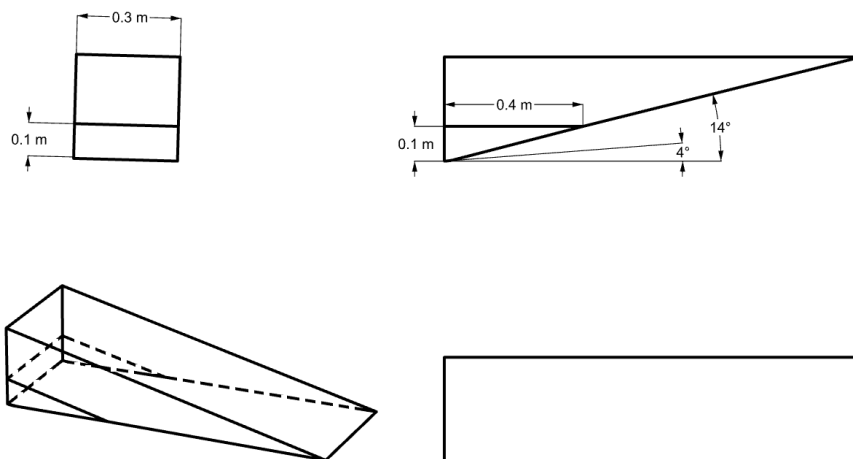
1  
2

Figure 23.

<b>Beam (m)</b>	0.3
<b>Length of water line (m)</b>	0.4
<b>Angle of attack in front (degree)</b>	14
<b>Angle of attack in stern (degree)</b>	4
<b>Draught (m)</b>	0.1

3  
4  
5

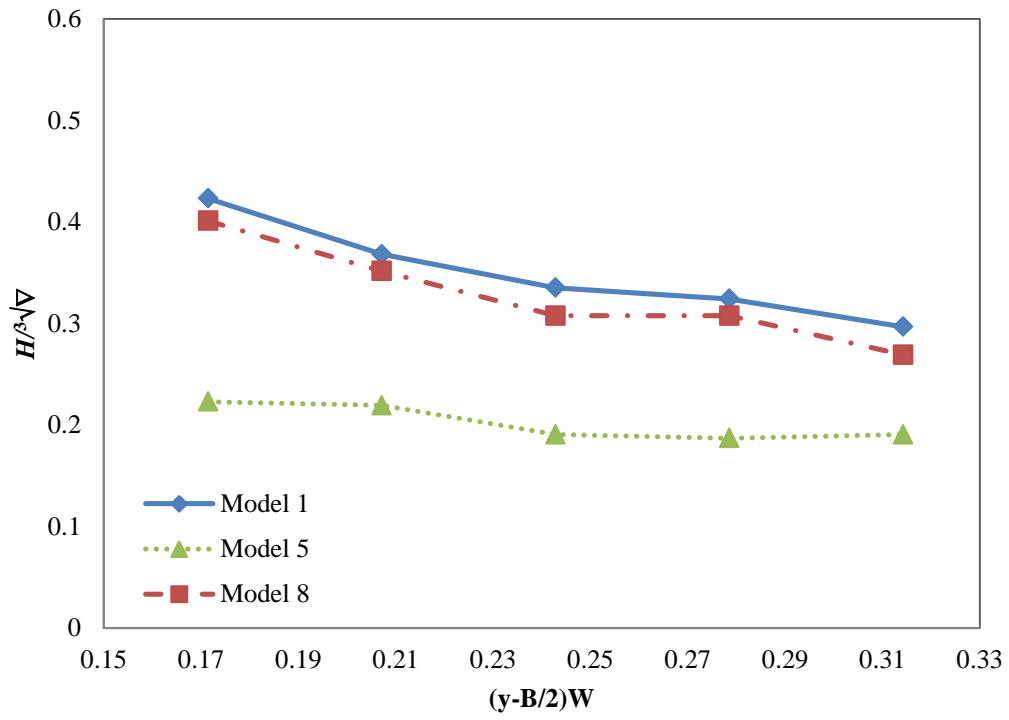
Table 5.



6

1

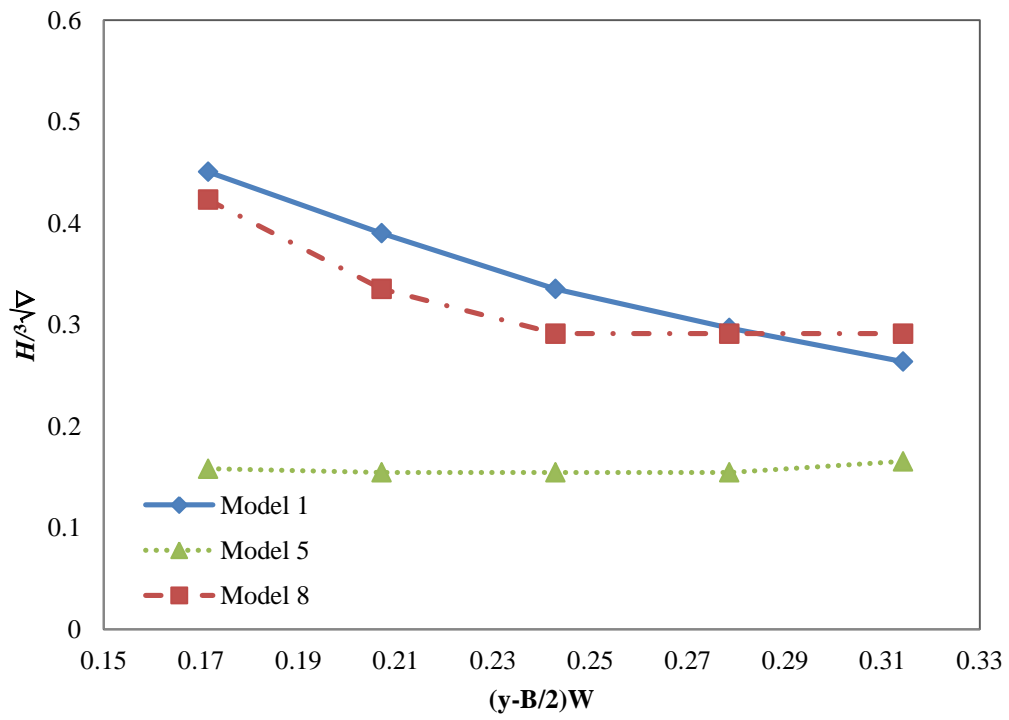
Figure 24.



2

3

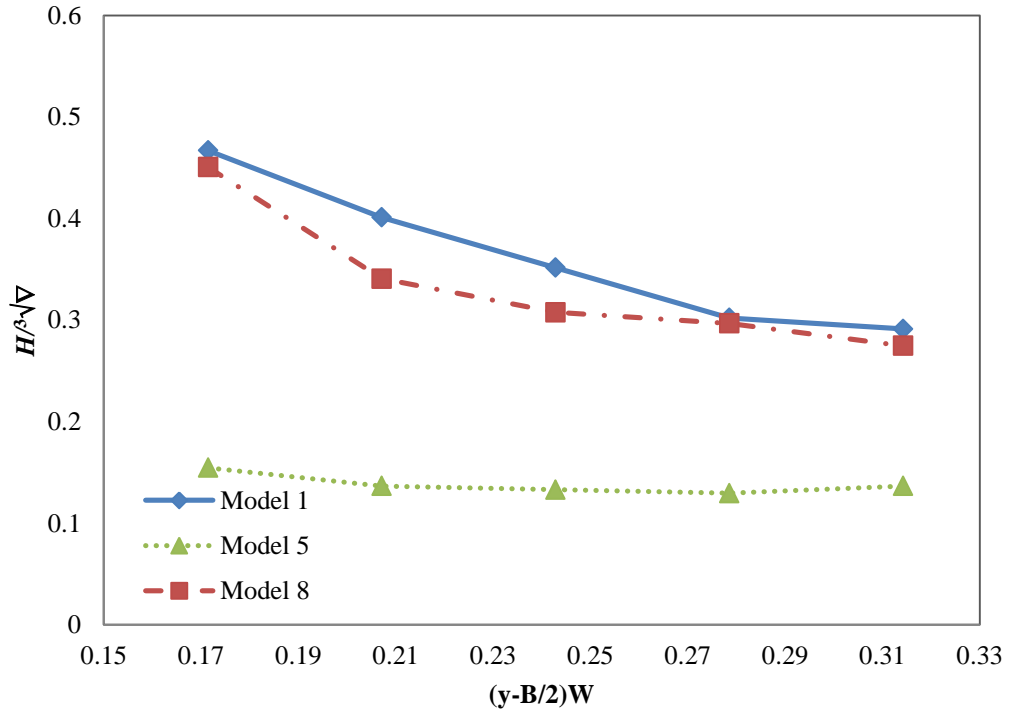
Figure 25.



4

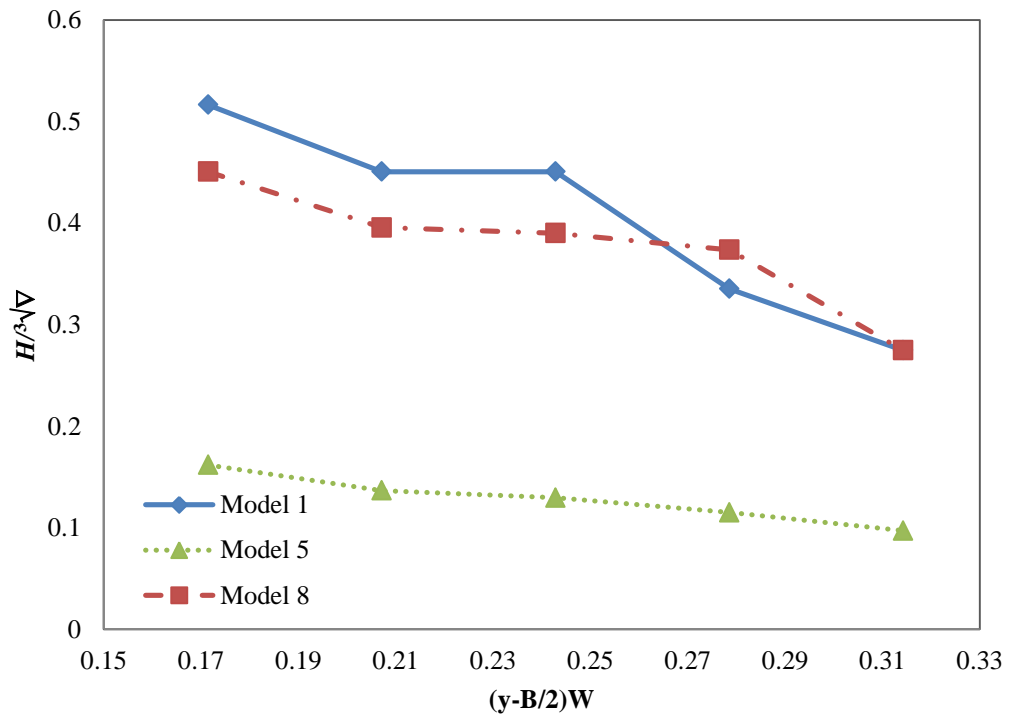
5

Figure 26.



1  
2

Figure 27.



3  
4  
5  
6  
7

Figure 28.

	V [m/s]			
	h [m]	1.66	1.99	2.66
Channel 1	0.4	0.838	1	1.343
Channel 2	0.45	0.79	0.947	1.266
Channel 3	0.5	0.75	0.9	1.2

Table 6.

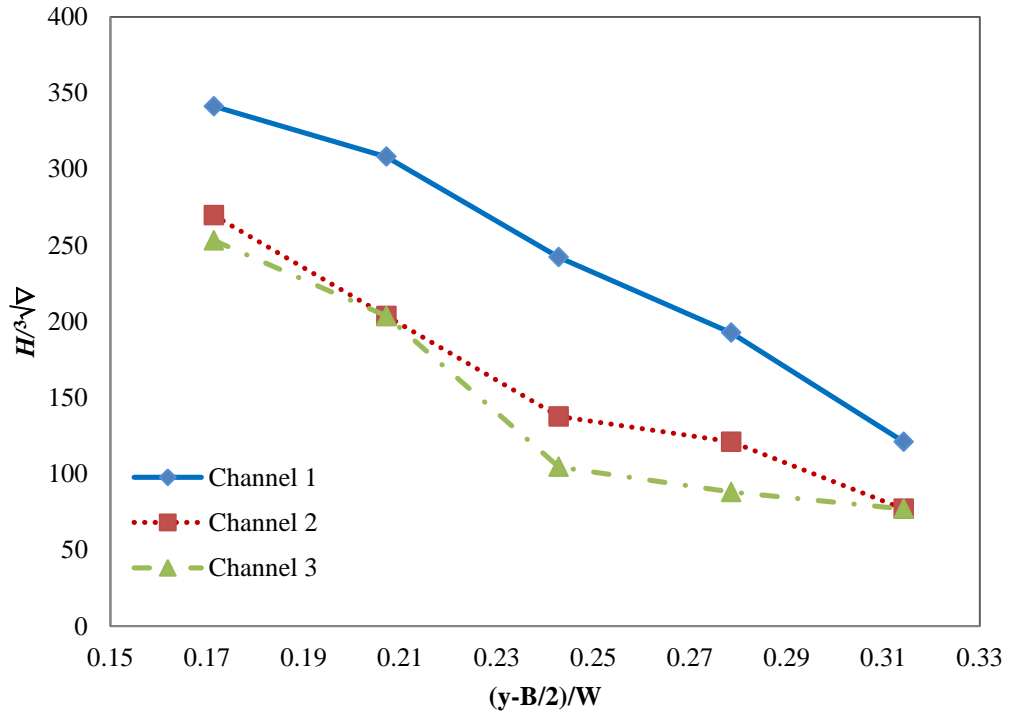
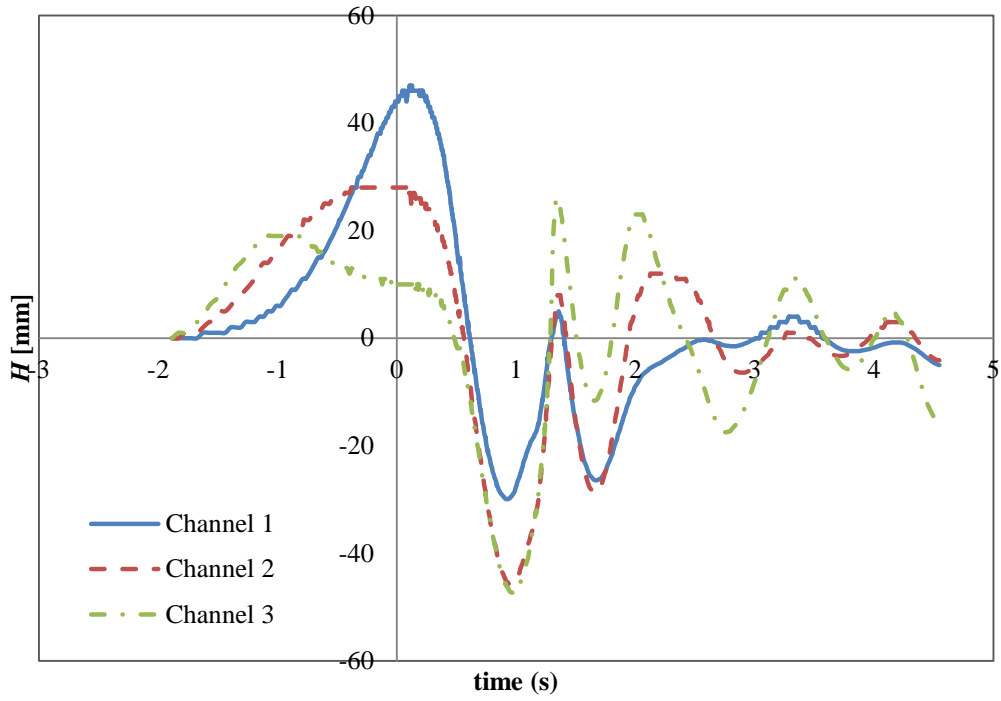
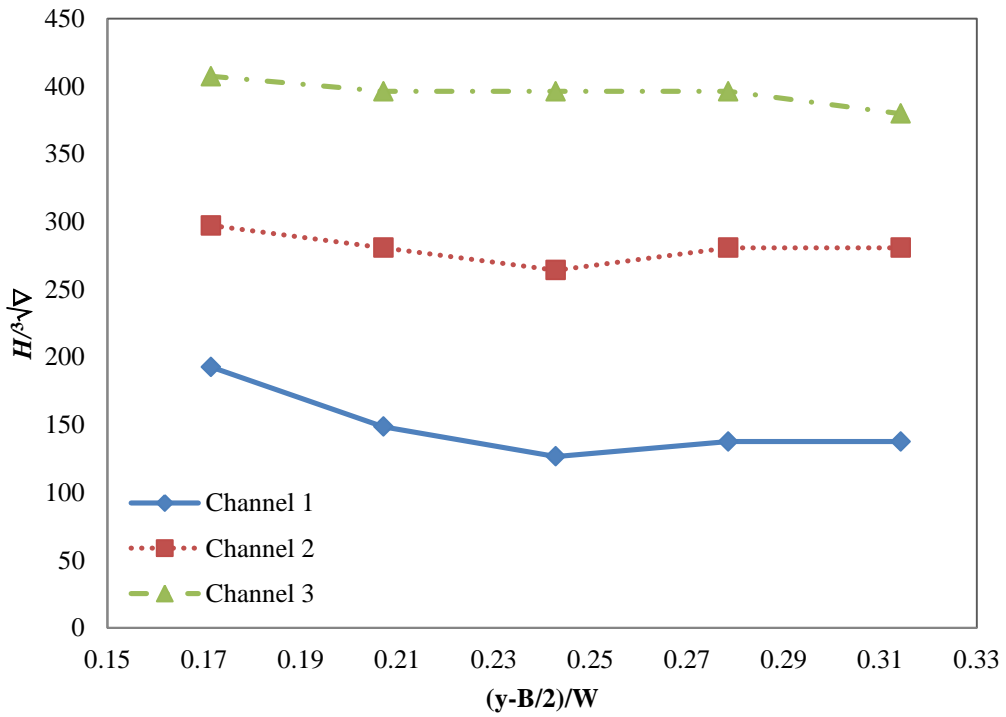


Figure 29.



1  
2  
3

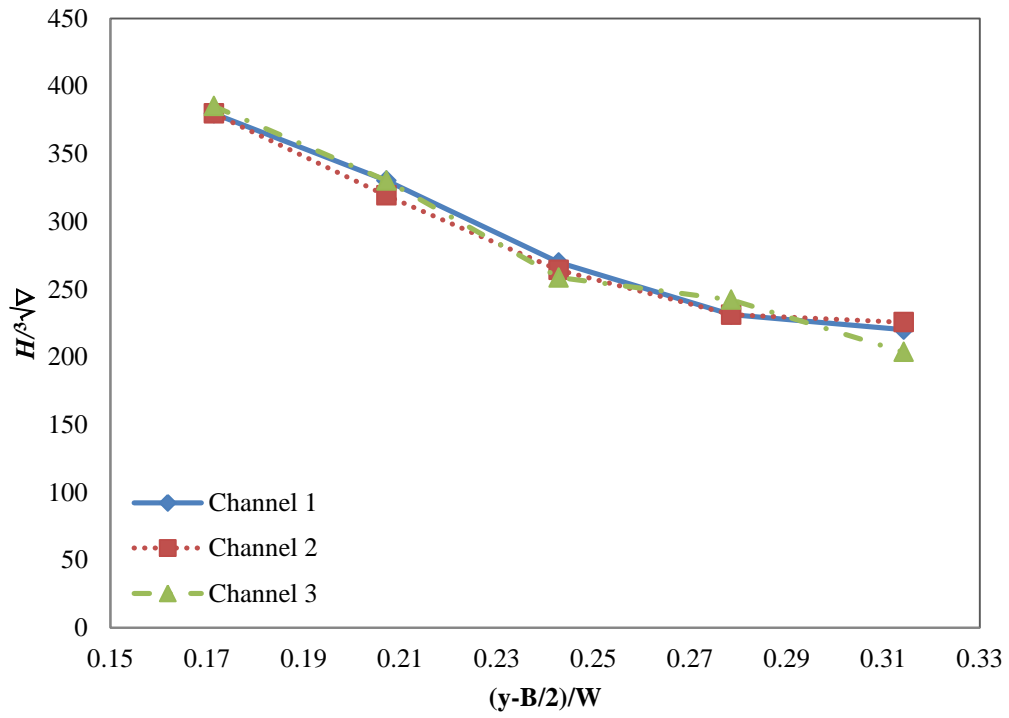
Figure 30.



4  
5

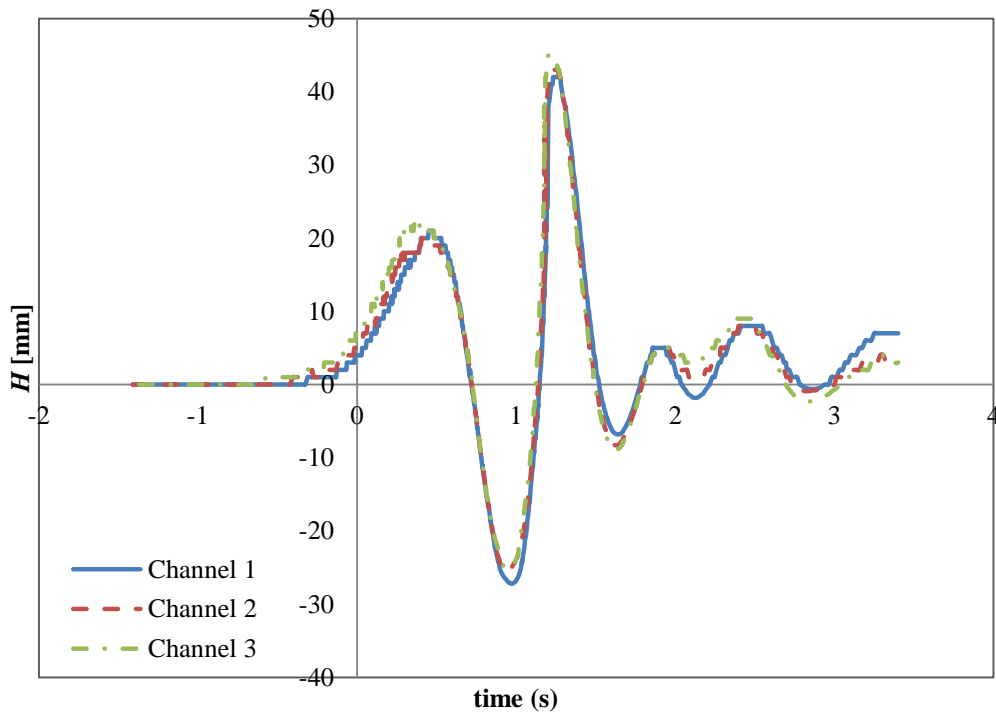
Figure 31.





1  
2  
3

Figure 32.



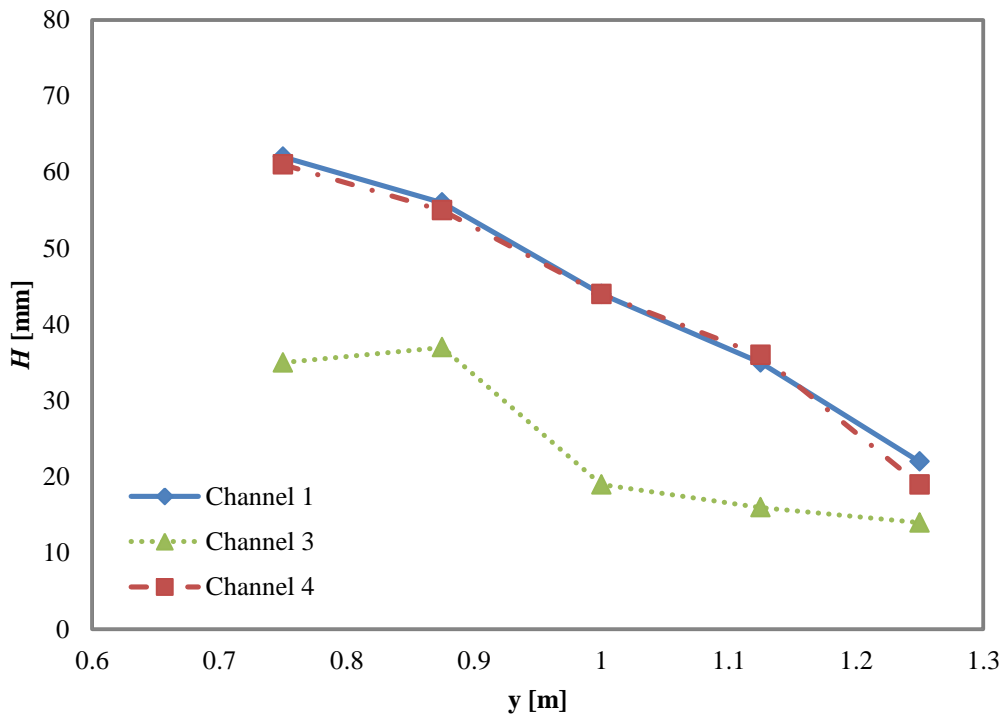
4  
5  
6  
7

Figure 33.

	Width (m)	Depth (m)	Blockage factor ( $\kappa$ )
<b>Channel 1</b>	3.5	0.4	0.0214
<b>Channel 3</b>	3.5	0.5	0.0171
<b>Channel 4</b>	4.375	0.4	0.0171

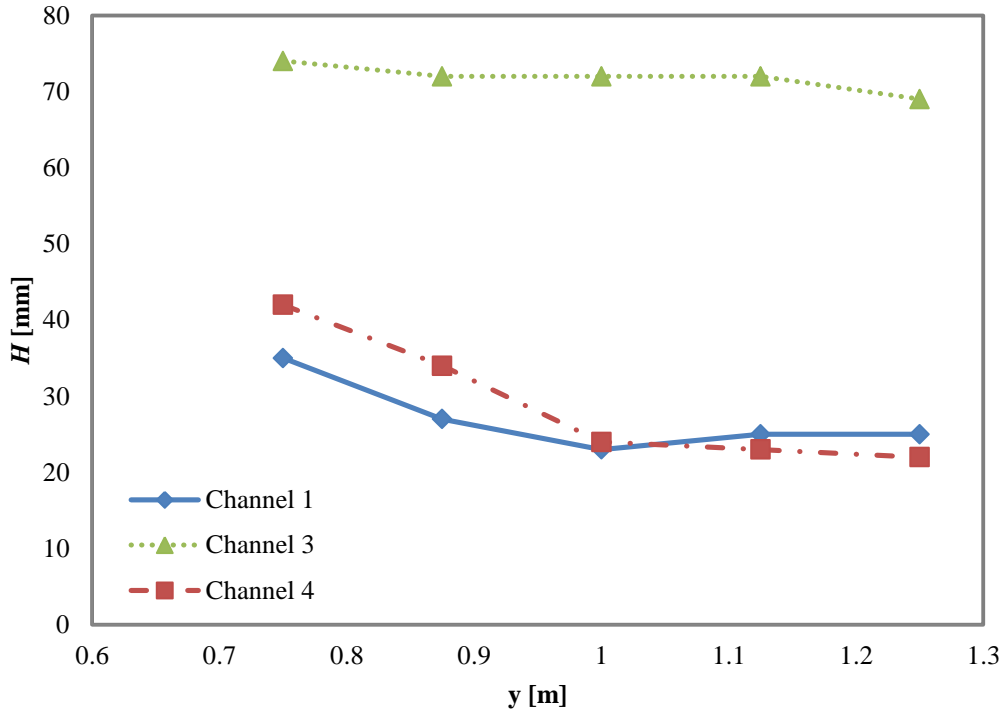
1  
2  
3

**Table 7.**



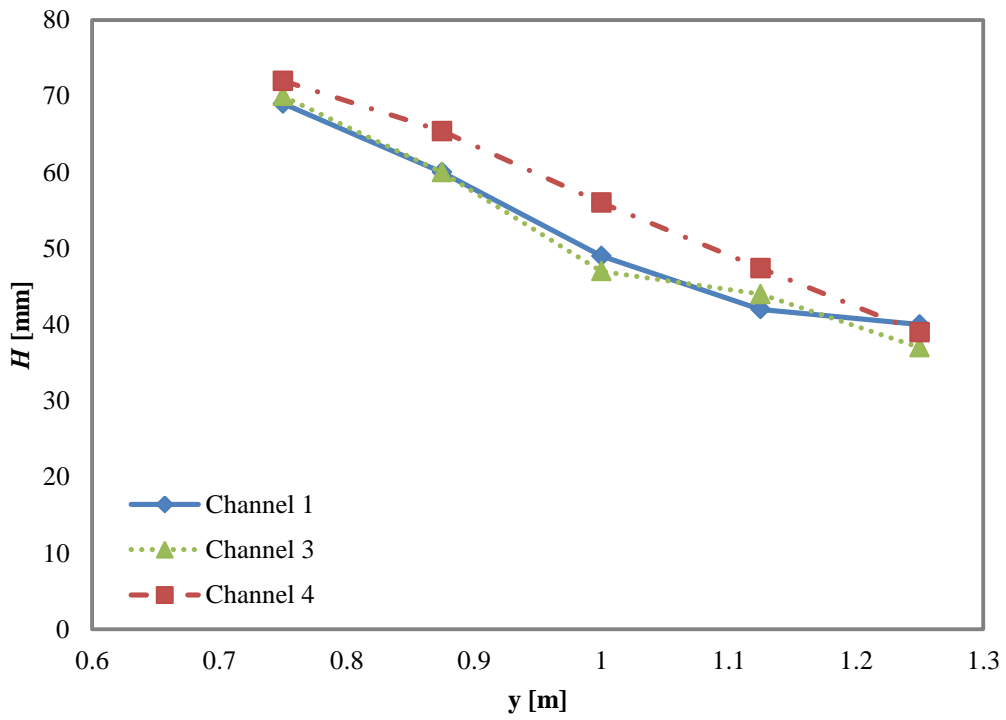
4  
5

**Figure 34.**



1  
2

Figure 35.



3  
4  
5  
6  
7

Figure 36.

1

2

### 3 **Appendices**

#### 4 **Abbreviations**

$\nabla$	Volume displacement	$H$	Wave height
$\kappa$	Blockage factor	$h$	Water depth
$\chi$	Longitudinal distance	LWL	Length of waterline
$A_c$	Channel cross section area	$p$	Pressure
AOA	Angle of attack	$V$	Speed of model
$A_s$	Model cross section area	$W$	Width of channel
B	Model beam	WP	Wave probe
$C_d$	Drag coefficient	$y$	Lateral distance
$C_l$	Lift coefficient	$y^*$	$y/W$
D	Model draught	$\rho$	Water density
$Fr_h$	Depth Froude number		

5